



Review

# Heterophase Polymorph of TiO<sub>2</sub> (Anatase, Rutile, Brookite, TiO<sub>2</sub> (B)) for Efficient Photocatalyst: Fabrication and Activity

Diana Rakhmawaty Eddy <sup>1,\*</sup>, Muhamad Diki Permana <sup>1,2,3</sup>, Lintang Kumoro Sakti <sup>1</sup>,  
Geometry Amal Nur Sheha <sup>1</sup>, Solihudin <sup>1</sup>, Sahrul Hidayat <sup>4</sup>, Takahiro Takei <sup>3</sup>, Nobuhiro Kumada <sup>3</sup>  
and Iman Rahayu <sup>1</sup>

<sup>1</sup> Department of Chemistry, Faculty of Mathematics and Natural Sciences, Universitas Padjadjaran, Sumedang 45363, West Java, Indonesia

<sup>2</sup> Integrated Graduate School of Medicine, Engineering, and Agricultural Sciences, University of Yamanashi, Kofu 400-8511, Japan

<sup>3</sup> Center for Crystal Science and Technology, University of Yamanashi, Kofu 400-8511, Japan

<sup>4</sup> Department of Physics, Faculty of Mathematics and Natural Sciences, Universitas Padjadjaran, Sumedang 45363, West Java, Indonesia

\* Correspondence: diana.rahmawati@unpad.ac.id; Tel.: +62-81322731173

**Abstract:** TiO<sub>2</sub> exists naturally in three crystalline forms: Anatase, rutile, brookite, and TiO<sub>2</sub> (B). These polymorphs exhibit different properties and consequently different photocatalytic performances. This paper aims to clarify the differences between titanium dioxide polymorphs, and the differences in homophase, biphasic, and triphasic properties in various photocatalytic applications. However, homophase TiO<sub>2</sub> has various disadvantages such as high recombination rates and low adsorption capacity. Meanwhile, TiO<sub>2</sub> heterophase can effectively stimulate electron transfer from one phase to another causing superior photocatalytic performance. Various studies have reported the biphasic of polymorph TiO<sub>2</sub> such as anatase/rutile, anatase/brookite, rutile/brookite, and anatase/TiO<sub>2</sub> (B). In addition, this paper also presents the triphasic of the TiO<sub>2</sub> polymorph. This review is mainly focused on information regarding the heterophase of the TiO<sub>2</sub> polymorph, fabrication of heterophase synthesis, and its application as a photocatalyst.

**Keywords:** titanium dioxide; heterophase; polymorph; anatase; rutile; photocatalysis



**Citation:** Eddy, D.R.; Permana, M.D.; Sakti, L.K.; Sheha, G.A.N.; Solihudin; Hidayat, S.; Takei, T.; Kumada, N.; Rahayu, I. Heterophase Polymorph of TiO<sub>2</sub> (Anatase, Rutile, Brookite, TiO<sub>2</sub> (B)) for Efficient Photocatalyst: Fabrication and Activity. *Nanomaterials* **2023**, *13*, 704. <https://doi.org/10.3390/nano13040704>

Academic Editor:  
Dorian A.H. Hanaor

Received: 14 January 2023

Revised: 7 February 2023

Accepted: 8 February 2023

Published: 12 February 2023



**Copyright:** © 2023 by the authors. Licensee MDPI, Basel, Switzerland. This article is an open access article distributed under the terms and conditions of the Creative Commons Attribution (CC BY) license (<https://creativecommons.org/licenses/by/4.0/>).

## 1. Introduction

Titanium dioxide, also known as titania, is a naturally occurring transition metal oxide of titanium with the chemical formula TiO<sub>2</sub> [1]. Titanium dioxide is the most effective and efficient semiconductor material as a photocatalyst, has good stability, and has high ultraviolet absorption compared to other materials [2–6]. In addition, TiO<sub>2</sub> is a commercially available materials for applications in various fields due to its wide availability, biocompatibility, and non-toxicity [7–9]. TiO<sub>2</sub> has a white colour which is used as a pigment in paints, printing inks, plastics, ceramics, and cosmetics [10–13]. TiO<sub>2</sub> is the most effective and efficient semiconductor material, and has also been reported in the photoelectrical devices [14,15]. TiO<sub>2</sub> also has electronic and optical properties that can be utilized in the field of photocatalysts [16], self-cleaning materials [17], and solar cells [18].

Titanium dioxide has many applications as a photocatalyst, for example, in hydrogen production [19–22], degradation of organic compounds [23–27], remediation of metal ions [28–30], and synthesis of organic compounds [31–34]. Most of the research on TiO<sub>2</sub> has been carried out to increase its photocatalytic efficiency [35]. Many studies have also been devoted to the synthesis of various forms of nanomaterials [36–38], engineered with doping [39–42] or composites [43–45].

TiO<sub>2</sub> exists naturally in three crystalline forms, anatase, rutile, and brookite [46–49]. Besides that, there is another polymorph, namely TiO<sub>2</sub> (B) [50,51]. These polymorphs exhibit different properties and, consequently, different photocatalytic performances [52]. In general, many studies have stated that anatase has the best photocatalytic activity [53]. However, in some cases, rutile is more active as a photocatalyst [54]. In addition, the binary mixture of TiO<sub>2</sub> polymorphs showed a significant increase in the rate of catalytic activity for several reactions. Among these phases, the binary phase of anatase and rutile is the most studied phase [55,56].

The main drawback of photocatalyst application is the high recombination rate of electrons and holes which will reduce the quantum efficiency and decrease the photocatalytic activity [57,58]. One way to overcome this problem is to use multiphase TiO<sub>2</sub> because it exhibits higher photocatalytic activity than single-phase due to the possible charge transfer generated between different TiO<sub>2</sub> polymorphs (with different levels of electronic bands), leading to an effective separation of charge carriers thereby preventing recombination of electrons and holes [59,60].

The TiO<sub>2</sub> heterophase can effectively stimulate electron transfer from one phase to another cause superior photocatalytic performance [61,62]. For example, TiO<sub>2</sub> P25 Degussa, which consists of ~20% rutile and ~80% anatase, is an excellent photocatalyst [63]. Several studies have succeeded in synthesizing TiO<sub>2</sub> heterophase which shows better photocatalytic abilities than pure anatase, namely, anatase/rutile [64] and anatase/brookite [65]. Growing research efforts have recently been devoted to new TiO<sub>2</sub> heterophase composites including anatase/TiO<sub>2</sub> (B) [66,67] and rutile/brookite [68], as well as the three-phase anatase/rutile/brookite [69] and anatase/rutile/TiO<sub>2</sub> (B) [70]. Wang et al. [71] reported a novel approach to fabricate heterophase anatase/TiO<sub>2</sub> (B) in which heterophase can be obtained at 550 °C. The results show that although in many cases the photocatalytic activity of TiO<sub>2</sub> (B) is lower than that of anatase, a suitable composition between anatase and TiO<sub>2</sub> (B) will lead to increased activity [72].

As described in detail by other researchers previously, the most obvious advantage of the multiphase photocatalyst is that it can promote electron–hole separation, thereby enhancing the photocatalytic activity of materials. Therefore, in the photocatalytic system, it is very important to synthesize a photocatalyst with a multiphase structure and high degradation efficiency. This review mainly addresses reports related to TiO<sub>2</sub> heterophase over the past 10 years, in which a wider field of research has been reported. This work aims to clarify the differences between titanium dioxide polymorphs, and the differences in homophase and heterophase (biphase and triphase) properties in various photocatalytic applications. This review includes information on TiO<sub>2</sub> polymorph heterophase, the fabrication of synthetic heterophase, and their applications as photocatalysts. This review ends with conclusions and perspectives, which may stimulate further development of the utility of TiO<sub>2</sub> heterophase. Review articles covering heterophase with thorough explanations have not been reported. Other reviews have focused on anatase and rutile [73–75] with other composite or doped materials [76–80].

## 2. Homophase TiO<sub>2</sub>

### 2.1. Photocatalysis Mechanism of TiO<sub>2</sub>

TiO<sub>2</sub> is a semiconductor material, which is a substance that lies between conductors (such as metals) and insulators (such as ceramics) [81]. In semiconductor, the distance between the position of the valence band (VB) and the conduction band (CB) determine the ability of the semiconductor material in the light absorption process and its oxidation–reduction ability [82–85]. In general, the photocatalytic reaction of TiO<sub>2</sub> includes several basic processes, such as the formation of charge carriers, separation, relaxation, capture, transfer, recombination, and transport [86–88]. This process must be thoroughly observed to understand the workings of TiO<sub>2</sub> photocatalysts and is useful for the development of new photocatalysts [89,90].

In general, the mechanism of photocatalysis using  $\text{TiO}_2$  is illustrated in Figure 1. When  $\text{TiO}_2$  material is subjected to photon irradiation with an energy greater than the band gap of  $\text{TiO}_2$ , the electrons in VB will be excited to CB resulting in holes in VB [91–95]. The process of photoexcitation of pairs of electrons ( $e^-$ ) and holes ( $h^+$ ) will participate in redox reactions with adsorbed species which will form superoxide radical anions ( $\bullet\text{O}_2^-$ ) and hydroxyl radicals ( $\bullet\text{OH}$ ), respectively, which will play a role in the degradation of organic pollutants in water [96–99]. Only photons with energies greater than the band-gap energy can excite electrons and drive reactions to occur. The activation of  $\text{TiO}_2$  by UV light can be written as Equations (1)–(3) [100–102]. In this reaction,  $h^+$  and  $e^-$  are strong oxidizing and reducing agents.

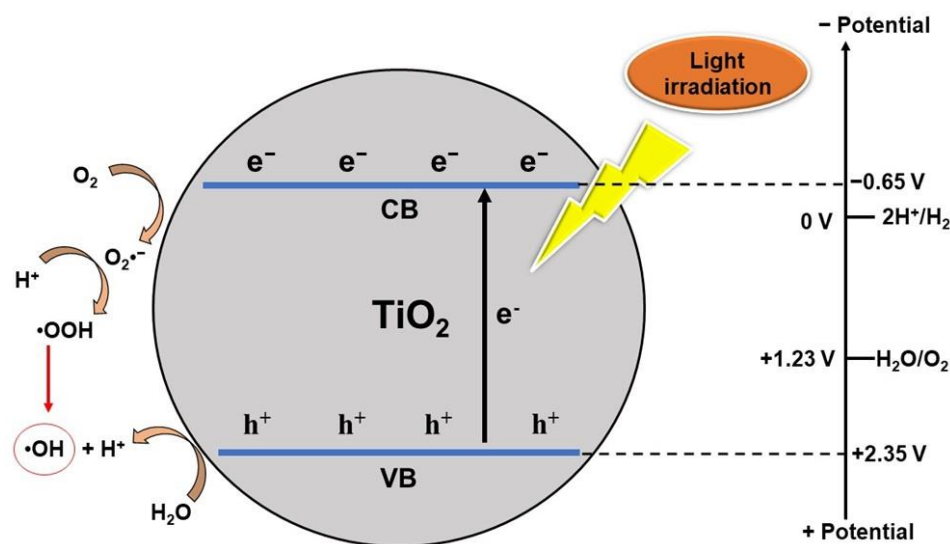


**Figure 1.** Schematic diagram of  $\text{TiO}_2$  photocatalytic principle.

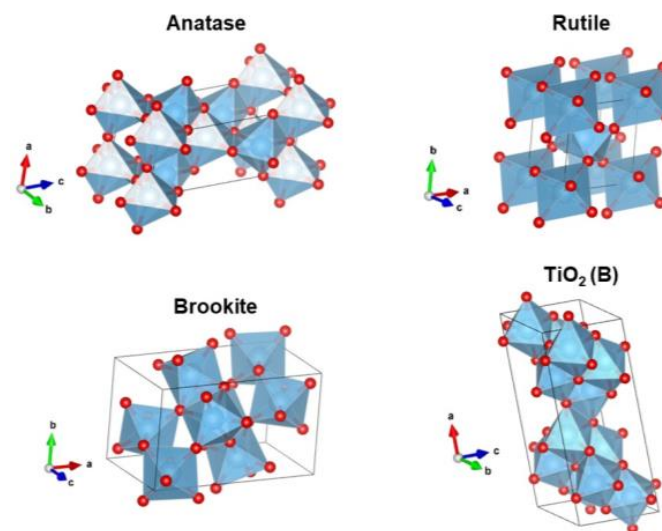
Reactive oxygen species (ROS) produced during the photocatalytic process vary greatly, mainly the ROS that is formed is the superoxide radical  $\text{O}_2\bullet^-$  and the hydroxyl radical  $\bullet\text{OH}$ . However, other species such as  $\bullet\text{OOH}$  and  $\text{H}_2\text{O}_2$  may be formed through further oxidation processes, dimerization, or disproportionation [103–105].

## 2.2. Phase of $\text{TiO}_2$

$\text{TiO}_2$  is widely available in nature as rutile, anatase, and brookite polymorphs; these three types are octahedral  $\text{TiO}_6$  with different distortions [106,107]. The structures of anatase, rutile, and brookite are shown in Figure 2 [108]. While rutile is a stable phase, both anatase and brookite are metastable phases. In addition, this brookite is difficult to synthesize, so it is rarely studied [109–112]. There is another polymorph found from  $\text{TiO}_2$ , namely  $\text{TiO}_2$  (B) [113–115]. The characteristics of the Ti-O bond determine the differences in the structural and electronic properties of the different  $\text{TiO}_2$  phases [116]. Table 1 shows the different properties of the  $\text{TiO}_2$  polymorph [117].

**Table 1.** Crystal structure and physical parameters of TiO<sub>2</sub> polymorphs.

Phase	Crystal System, Space Group	Lattice Parameter	Density (g/cm <sup>3</sup> )	Band Gap Energy (eV)	Ref.
Brookite	Ortorombik, <i>Pbca</i>	$a = 9.148 \text{ \AA}$ $b = 5.447 \text{ \AA}$ $c = 5.145 \text{ \AA}$ $V = 257.38 \text{ \AA}^3$	4.12	3.14–3.31	[117]
Rutile	Tetragonal, <i>P4<sub>2</sub>/mmm</i>	$a = b = 4.594 \text{ \AA}$ $c = 2.959 \text{ \AA}$ $V = 62.45 \text{ \AA}^3$	4.25	3.02–3.04	[117]
Anatase	Tetragonal, <i>I4<sub>1</sub>/amd</i>	$a = b = 3.784 \text{ \AA}$ $c = 9.515 \text{ \AA}$ $V = 136.24 \text{ \AA}^3$	3.89	3.20–3.23	[117]
TiO <sub>2</sub> (B)	Monoclinic, <i>C2/m</i>	$a = 12.179 \text{ \AA}$ $b = 3.741 \text{ \AA}$ $c = 6.525 \text{ \AA}$ $\beta = 107.054$ $V = 284.22 \text{ \AA}^3$	3.73	3.09–3.22	[113]

**Figure 2.** Crystal structure of TiO<sub>2</sub> anatase, rutile, brookite, and TiO<sub>2</sub> (B).

In general, anatase showed higher photocatalytic activity than rutile. However, the reason for the difference in photocatalytic activity between these phases is still being debated [118,119]. Zhang et al. [120] showed that anatase is a semiconductor with an indirect band gap, while rutile and brookite are included in the category of direct band gap semiconductors. In addition, photocatalytic effects such as organic pollutant decomposition will be successful if the semiconductor material has a band gap energy of redox potential at the hole that is VB positive enough to produce hydroxyl radicals and electrons in CB, which must be negative enough to produce superoxide radicals ( $E_0(\text{H}_2\text{O}/\bullet\text{OH}) = 2.8 \text{ V vs. NHE}$ ) and ( $E_0(\text{O}_2/\text{O}_2^{\bullet-}) = -0.28 \text{ V vs. NHE}$ ). Figure 3 shows the band gap energies of anatase, rutile, and brookite TiO<sub>2</sub> [121–123].

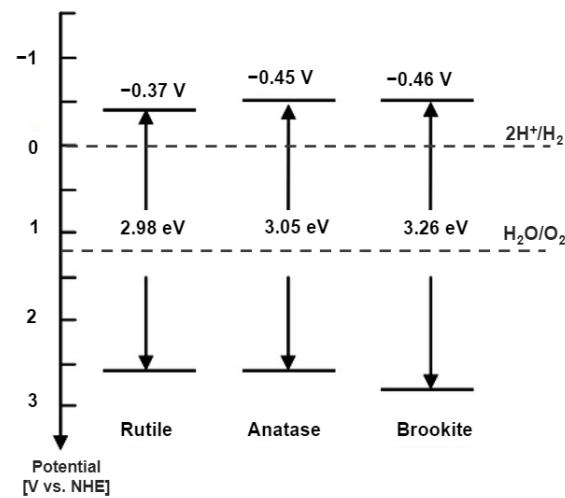


**Figure 3.** Bandgap energies, VB, and CB for anatase, rutile, and brookite on the potential scale (V) versus the normal hydrogen electrode (NHE).

### 2.2.1. Anatase

Anatase polymorph has better photocatalytic activity than other  $\text{TiO}_2$  polymorphs [124–128]. Anatase has a larger band gap than rutile. This increases the oxidizing ability and facilitates electron transfer. Recent results show that the anatase has a lower conduction band than the rutile [129]. Moreover, the indirect band gap of the anatase form is smaller than the direct band gap. Thus, the indirect band gap is used for the photocatalysis process of the anatase form. For rutile, on the other hand, the fundamental band gap of indirect band gap is very similar to the direct band gap. Thus, the rutile type tends to excite electrons in a direct band gap. Indirect band gap materials generally exhibit a longer charge carrier lifetime compared to direct band gap materials [130–133], thus making anatase have better activity in most cases compared to rutile and brookite.

Anatase has a much wider specific surface area, so it has more active sites than rutile. Anatase also has a higher oxygen vacancy concentration than rutile, which is the reason for anatase's higher charge separation efficiency [134]. The adsorption affinity of anatase for organic compounds is higher than that of rutile, and anatase shows a lower recombination rate than that of rutile because of its higher hole-trapping rate [135]. The adsorption affinity is defined as the equilibrium ratio of the solid-phase concentration to the liquid-phase solute concentration, also known as adsorption equilibrium constant [136]. However, even though it has better photocatalytic activity, the single anatase phase has low thermodynamic stability when compared to the rutile phase, so it can only be synthesized in several types of synthesis [137,138].

Bubacz et al. [139] synthesized anatase  $\text{TiO}_2$  with  $\text{TiOSO}_4$  precursor in ammonia water as a phenol degradation and azo dye. The decreased concentrations of the dye and phenol was measured by UV/VIS spectroscopy and a TOC analyzer. Polycrystalline of anatase was produced with a crystalline size of 12.7–13.0 nm and a particle size of 195.7 nm. The material produces satisfactory activity with an optimum pH of 6.5. In addition, Etacheri et al. [140] synthesized anatase with a band gap that can be reduced (without doping) and can work in visible light. This is achieved by generating oxygen in situ via the thermal decomposition of the peroxo–titania complex ( $\text{H}_2\text{O}_2\text{-TiO}_2$ ). The increased strength of the Ti–O–Ti bond and the maximum shift of VB are responsible for the stability in high temperature and visible light activity (Figure 4).

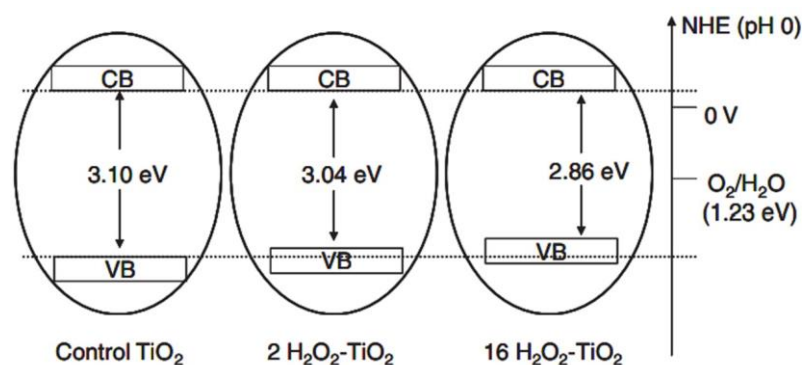


**Figure 4.** Mechanism of band gap narrowing for peroxy-titania (anatase) complex. Reproduced with permission from [140]. Copyright John Wiley and Sons, 2011.

In the report of Lv et al. [141], anatase is modified using fluorine as a shape guide for surface modification. This modification produces various morphological forms such as nanotubes, titania sheets with {001} high-energy facets, and hollow spheres. This form results in increased diverse photocatalytic activity. In this regard, regarding the effect of fluoride on the structure and photocatalytic activity of TiO<sub>2</sub>, many questions remain open. In another report, Wang et al. [142] reported the differences in the photocatalytic activity ability between anatase and rutile mesopores. Mesoporous anatase results in long-lived electron generation and allows for efficient electron transfer. Meanwhile, mesoporous rutile is substantially less efficient and more reversible than anatase.

### 2.2.2. Rutile

The rutile phase becomes an attractive polymorph TiO<sub>2</sub> for photocatalytic applications because it can absorb UV light near the visible region. The band gap of rutile is 3.0 eV, lower than that of anatase (3.2 eV). However, the rutile phase has not been widely studied as a photocatalyst because of its lower photocatalytic activity than anatase. Its low specific surface area, fast recombination, and the positive location of its minimum conduction band make it have a poorer reducing ability than anatase [143–147].

Rutile is the most stable TiO<sub>2</sub> polymorph and is easily produced at high temperatures. However, rutile has rarely been studied as a photocatalyst for the oxidation of dyes/organic compounds, due to poor oxygen uptake due to the lower valence band position compared to anatase [148]. In the research by Wang et al. [149], rutile was successfully synthesized using low temperatures. Pure rutile was synthesized by hydrolysis of an aqueous TiCl<sub>4</sub> ethanol solution at 50 °C. The results show that rutile synthesized at low temperatures exhibits much higher photocatalytic activity than commercial P25 photocatalysts in the degradation of rhodamine B. Applications of rutile photocatalysis include water separation. In contrast to anatase, rutile allows preferential water oxidation, which is useful for the construction of Z-scheme water separation systems [150]. In addition, in another study, rutile nanoparticles with large specific surface areas and abundant oxygen vacancies were designed for photocatalytic nitrogen fixation [151]. Meanwhile, in a study conducted by Yurdakal et al. [152], rutile was used for the selective oxidation of aromatic alcohols to aldehydes in an aqueous suspension.

The photocatalytic abilities of rutile and anatase were compared by Jung and Kim [153] to stearic acid and measured the rate of decrease in the integrated absorbance of the ensemble of the C–H stretching vibrations using FTIR spectroscopy. The results show that although rutile nanoparticles have a higher specific surface area than anatase nanoparticles, the photocatalytic properties of rutile nanoparticles are much lower than those of anatase nanoparticles. This is attributed to the intrinsic radiative recombination of photogenerated electrons and holes in rutile. However, other studies have shown that the presence of the vacancy-oxygen defect (VO) in rutile can significantly increase the ability of photocatalytic activity. VO is known to suppress the charge recombination process [154]. Although in

many studies anatase shows higher activity, in some cases, rutile can be superior [155]. For example, the research by Zhang et al. [156], compared the photocatalytic activity of anatase, rutile, and brookite for Rhodamine B (RhB) degradation. The results show that rutile provides a faster photocatalytic reaction rate than anatase for the same particle size and specific surface area.

### 2.2.3. Brookite

Brookite has an orthorhombic crystal structure with the *Pbca* space group [157]. Brookite will turn into rutile at high temperatures. This conversion can occur directly to rutile or through the formation of anatase first. This depends on several factors such as crystallite size, size distribution, and crystallite contact area. [158]. For crystal sizes larger than 11 nm, brookite is more stable than anatase, while for sizes larger than 35 nm, rutile is the most stable phase [159]. Xie et al. [160] synthesized pure-phase brookite by hydrothermal method using  $\text{Ti}(\text{SO}_4)_2$  as the precursor. Phase formation is achieved by hydrothermal treatment at 180 °C [161]. Kandiel et al. [162] observed that a direct transformation of anatase and brookite to rutile was observed, while in the case of anatase–brookite mixture, anatase changed first to brookite and then to rutile.

The photocatalytic activity of brookite was studied by Khan et al. and its activity is highly dependent on the level of disability. The results of the DFT calculations show that the  $\text{Ti}^{4+}$  defect is the main defect in increasing the photocatalytic activity of brookite [163,164]. One of the main reasons for the different catalytic performances of the  $\text{TiO}_2$  polymorph is the depth of charge carrier trapping. Electrons in brookite are trapped in shallow traps and not photogenerated, which reduces the amount of free electron, but on the other hand, this extends the life span of hole [165].

Bellardita et al. calculated the absolute crystallinity of brookite. This value was calculated from the ratio between the full width at half maximum (FWHM) intensity peak XRD pattern (121) of brookite and peak (111) of  $\text{CaF}_2$  as an internal standard. The results showed that crystallinity had a positive effect on the oxidation of 4-nitrophenol and 4-methoxybenzyl alcohol [166]. Choi et al. [167] synthesized pure brookite  $\text{TiO}_2$  films as a photocatalyst. The brookite phase was synthesized on titanium foil using a hydrothermal reaction. The results show that the brookite phase exhibits significantly higher photoactivity among the  $\text{TiO}_2$  polymorphs, despite its smaller specific surface area compared to anatase [168]. Tetramethylammonium (TMA) can be degraded in pure anatase and brookite phases, but not in rutile, where TMA concentration was measured by ion chromatograph [167].

### 2.2.4. $\text{TiO}_2$ (B)

$\text{TiO}_2$  (B) is a polymorph of titanium dioxide discovered in 1980 which was prepared from the hydrolysis of  $\text{K}_2\text{Ti}_4\text{O}_9$  followed by heating at 500 °C.  $\text{TiO}_2$  (B) has a host covalent framework of  $\text{Na}_x\text{TiO}_2$  bronze [169]. In 2004, Armstrong et al. [115] successfully prepared  $\text{TiO}_2$  (B) nanowires. The synthesis was carried out involving a hydrothermal reaction between NaOH and  $\text{TiO}_2$ , followed by acid washing and heating at 400 °C. The synthesized  $\text{TiO}_2$  (B) has the potential to be a material in lithium-ion batteries because it has the advantage of having a relatively open structure. Therefore, it is an excellent host for Li intercalation [170–173].  $\text{TiO}_2$  (B) nanoparticles were also developed with various sizes. The small particle size causes the dimensionality reduction to increase the amount of Li and hence the charge that can be stored [174].

The use of  $\text{TiO}_2$  (B) as a photocatalyst was carried out by Chakraborty et al. [175]. The results show that  $\text{H}_2\text{Ti}_5\text{O}_{11}\cdot\text{H}_2\text{O}$  is a prerequisite for the formation of  $\text{TiO}_2$  (B) phase. The photocatalytic activity of  $\text{TiO}_2$  (B) showed 1.35 and 1.95 times higher in decomposing 4-chlorophenol than Degussa P25 and 25 nm sized anatase nanoparticle. This is due to the high crystallinity of  $\text{TiO}_2$  (B). In addition, in other studies,  $\text{TiO}_2$  (B) doped with  $\text{Ti}^{3+}$  provided increased photocatalytic performance in rhodamine B (RhB) decomposition, which was measured using a UV spectrophotometer and hydrogen evolution, which was

measured using gas chromatography. The RhB degradation rate is  $\sim 6.9$  and the hydrogen evolution rate is 26.6 times higher compared to titanium dioxide nanoparticles [176].

### 2.3. Disadvantages of TiO<sub>2</sub> Homophase Photocatalysis

TiO<sub>2</sub> has great potential as a photocatalyst for the degradation of organic pollutants and microorganisms. However, in practice, there are many limitations, namely, high  $h^+$  and  $e^-$  recombination rates, low adsorption capacity, and low thermal stability of the anatase TiO<sub>2</sub> phase (Figure 5). TiO<sub>2</sub> has a wide band gap of 3.0–3.2 eV, meaning this photocatalyst mainly absorbs ultraviolet photons, while indoor lamps only emit visible light photons [177,178]. This causes the use of indoor photocatalysts such as disinfection to be very limited because they require UVA irradiation. Strategies that can be implemented to overcome this challenge include adding metals (Cu, Ag, Eu, Fe, Zn, and La) [179–182], adding non-metallic dopants (N, F, S, and C) [183–186], or the use of the photon induction method [187].

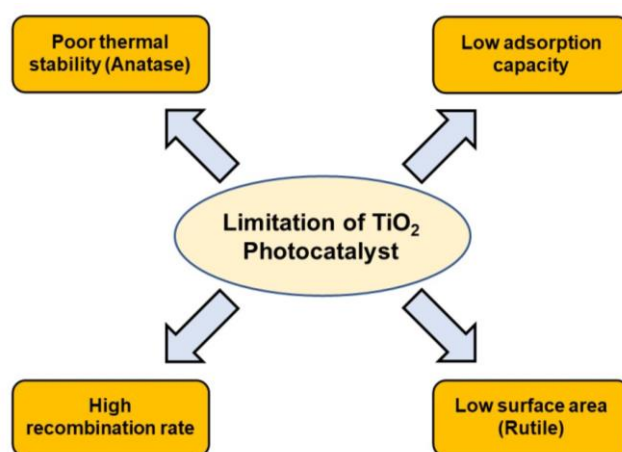


Figure 5. Limitations of TiO<sub>2</sub> as a photocatalyst material.

The crystallite size and phase of TiO<sub>2</sub> are aspects that affect the photonic efficiency and recombination dynamics in the photocatalytic process. Samples with a single anatase phase showed a high percentage of recombination due to the influence of crystallographic and microstructural parameters [188]. Meanwhile, samples with a mixed phase, such as anatase/rutile, have a more prominent crystallography and microstructure between anatase (011) and (110) rutile, which causes a decrease in the recombination rate due to the presence of hole and electron transfers [189]. Meanwhile, in the single rutile phase, there is a decrease in the formation rate of  $\bullet OH$  and  $e^-$  due to the less efficient formation of  $\bullet OH$  species during the oxidation of water on the rutile particles, as well as the shorter lifetime and lower reactivity of  $e^-$  in the single rutile phase. This phenomenon indicates that the photocatalytic synergy associated with anatase/rutile mixtures is not always present, but depends on the relationship between the fermi level of the anatase and rutile particles and the characteristics of the particles [190]. Photocatalytic junctions, especially type-II heterojunctions between semiconductors, are considered a potential pathway to improve photocatalytic performance [191]. The homojunction heterophase that exploits polymorphism has potential advantages. It has homogeneous components and nearly perfect lattice matching, and they can conduct efficient charge transfer at the interface [192].

### 3. Heterophase TiO<sub>2</sub> in Photocatalysts

#### 3.1. Photocatalysis Mechanism of TiO<sub>2</sub> Heterophase

TiO<sub>2</sub> with mixed phases such as anatase and rutile showed better photocatalytic activity than TiO<sub>2</sub> with 100% anatase phase. This increase in activity generally comes from the interaction between the two forms; the interaction reduces recombination due to a bulk structure of anatase/rutile. This mixed phase has an interfacial electron trapping site that enhances the photocatalytic activity of TiO<sub>2</sub> [193]. Meanwhile, in the anatase structure, the oxidation process is limited, while in contrast to the rutile structure, the reduction process is limited. Thus, when it is TiO<sub>2</sub> with the mixed phase, the oxidation-reduction process can be accelerated [194]. This is illustrated in Figure 6. When different phases of TiO<sub>2</sub> are mixed, the rate of recombination is reduced, the lighting efficiency is increased, and the energy band gap can be activated by light with energies lower than UV [135]. Due to its high activity, P25 Degussa, a commercial TiO<sub>2</sub>, is frequently used as a benchmark in photocatalytic processes. It has a mixed phase of anatase and rutile with a ratio of 80% and 20%, respectively [195].

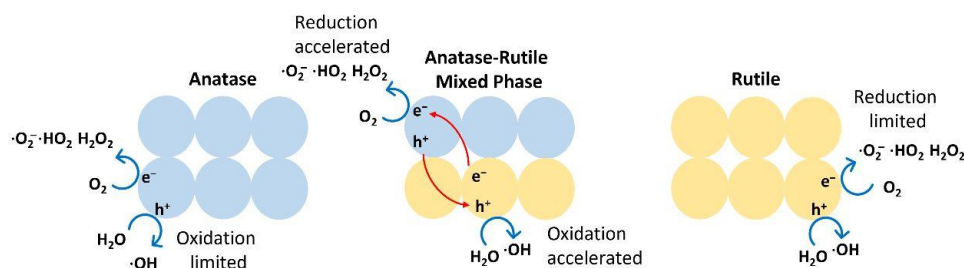


**Figure 6.** Mechanism of photocatalysis in anatase, rutile, and anatase–rutile heterophase.

At semiconductor heterojunctions, energy bands of two different materials come together, leading to an interaction. Both band structures are positioned discontinuously from each other, causing them to align close to the interface [196]. This alignment is caused by the discontinuous band structures of the semiconductors when compared to each other and the interaction of the two surfaces at the interface [197]. In research by Scanlon et al. [198], there are signs that when there is contact, the valence band energy and conduction band energy are higher in the rutile phase than in the anatase phase. Electrons will go to the anatase because of the lower conduction band minimum energy, and holes will move to the rutile because of the higher valence band maximum energy, according to the alignment of the bending energy bands at the anatase/rutile interface. Then, the holes in the valence band will react with water to generate hydroxyl radicals, while the electrons in the conduction band will concurrently react with oxygen to generate superoxide anions [199,200]. Figure 7 shows that the energy band changes at the interface of the anatase/rutile heterojunctions can lead to electron–hole separation and band bending until the Fermi levels of the anatase and rutile are aligned, and the density of the heterojunction and the toxicity of the nanoparticles can be determined by the degree of the band bending. The degree of band bending can be used to experimentally show that the heterojunction density of the TiO<sub>2</sub> mixed phase is theoretically proportional to the quantity of electron–holes at the heterojunction interface. Heterojunction density is the local density of state and charge density for heterojunction semiconductor (usually composites), which is calculated using computational software such as the Vienna ab initio simulation package (VASP) and Cambridge Sequential Total Energy Package (CASTEP) [201]. Furthermore, the ROS generated during the photocatalytic process and its potential in the oxidation process can be estimated by the band bending value [202]. Band bending value or degree of band bending is proportional to the amount of accumulated electrons or holes that depend on the density of heterojunction; this value can reflect the density of heterojunction in mixed-phase TiO<sub>2</sub> [203].

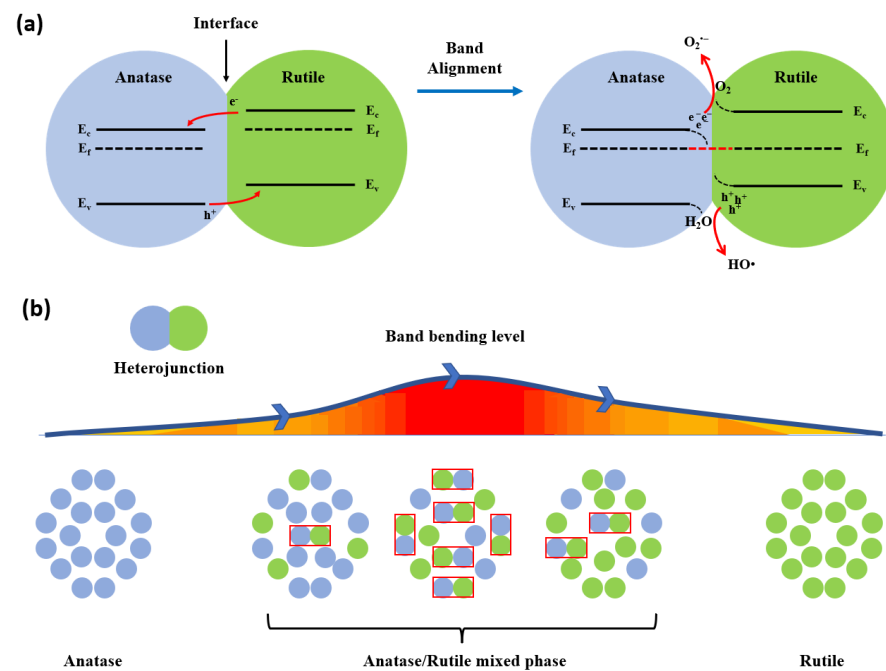


**Figure 7.** Heterojunction of mixed-phase  $\text{TiO}_2$  nanoparticles: (a) alignment of the conduction band and valence band between the rutile and anatase phases, which causes the separation of electron holes at the heterojunction; and (b) heterojunction density variations during the transformation of the anatase phase to rutile.

### 3.2. Computational Study of Heterophase $\text{TiO}_2$

Surface structures and interfacial sections are very important for photocatalytic processes because these points are considered as the focus of transfer and trapping of charge carrier species [204,205]. The possible arrangement at the interfacial point between anatase and rutile was analyzed by stacking the atomic layers of the anatase (011) plane and the (110) rutile plane [189]. In a study by Denkins et al. [206], two plates were prepared, one anatase and one rutile, each 30 Å thick, separated from each other by 5 Å. Then, MD simulations were carried out for 400 ps at 1300 K. An illustration of the initial and final structures is shown in Figure 8. As shown, a vacuum distance of about 25 Å is present to minimize interactions between non-interfacial surfaces.

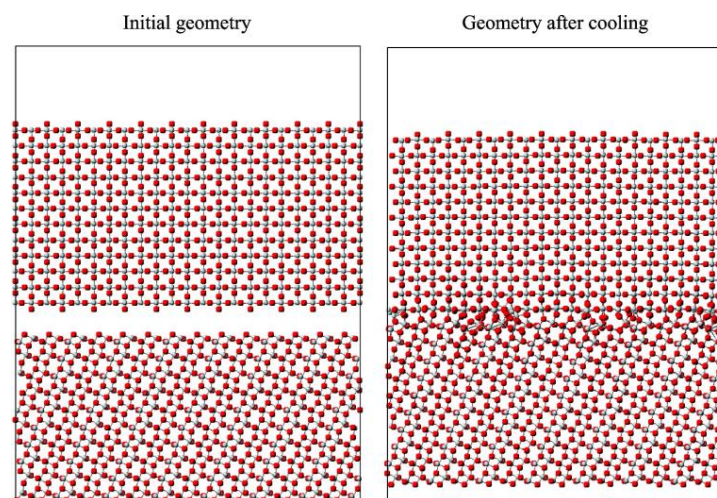


**Figure 8.** Interface formation between rutile (110) and anatase (101) before and after the cooling steps. Reproduced with permission from [206]. Copyright American Chemical Society, 2007.

The band gap of the structure of the TiO<sub>2</sub> mixture measured using HSE06 is around 3.0 eV which comes from the alignment band between the anatase (3.5 eV) and rutile (3.2 eV) phases [207]. The quantum size effect is responsible for the distinction in the band-gap values (approximately 0.2 eV) of each phase. The energy level of the Ti d orbitals can be adjusted by various coordination configurations, which makes this plausible. Additionally, a significant component in determining the photocatalytic activity linked to geometric and electrical structures is the absorption of photons from a semiconductor photocatalyst [208]. There is no significant change for the absorption curves of the mixed structure compared to the individual components of anatase and rutile. It shows that there is little orbital overlap and little electronic transition between rutile and anatase, and that direct electronic infusion of rutile into anatase hardly ever occurs during the excitation process. The structural changes that form the interface have no significant effect on the absorption of light by mixed-phase TiO<sub>2</sub> and the optical absorption of this structure occurs in the anatase and rutile phases, respectively [205]. In another study, anatase/rutile (A/R) and interlayer amorphous (Am) films A/Am/R were synthesized using atmospheric pressure chemical vapor deposition (APCVD) to produce the absorption and bandgap shown in Figure 9. The gap energy of the band for the anatase/rutile heterojunction (2.78 eV) appears red-shifted from the pure component [209].

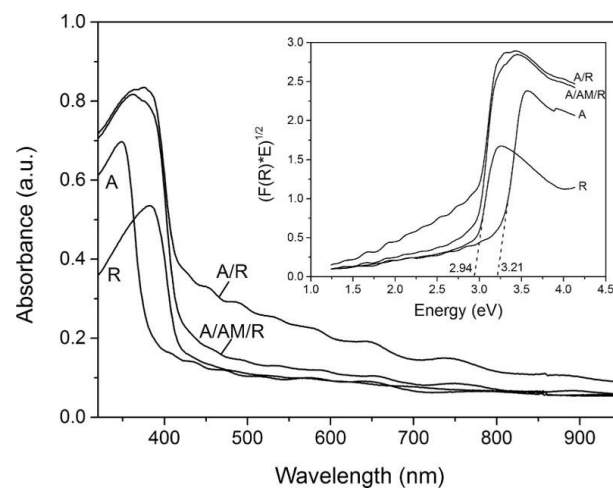


**Figure 9.** Absorption spectra of anatase (A), rutile I, multilayer films before (A/Am/R) and after (A/R) heat treatment at 500 °C for 10 h. Inset: Tauc plots showing approximate bandgap energy values of the A,R crystalline phases. Reproduced with permission from [209]. Copyright John Wiley and Sons, 2014.

### 3.3. Fabrication Methods of Heterophase TiO<sub>2</sub>

#### 3.3.1. Sol–Gel Method

In general, the sol–gel process involves a system transition from a liquid ‘sol’, which is mostly in the colloidal form, to a solid ‘gel’ phase. The starting materials used in the manufacture of ‘sol’ in the synthesis of TiO<sub>2</sub> are usually metal alkoxide compounds such as titanium tetraisopropoxide (TTIP) and inorganic metal salts such as TiCl<sub>4</sub> [210–212]. Arnal et al. [213] prepared titania by the sol–gel method from TiCl<sub>4</sub> in diethyl ether, at 110 °C, to produce anatase. Meanwhile, for TiCl<sub>4</sub> with ethanol, it leads to rutile as early as 110 °C, whereas the reaction of tert-butyl alcohol at 110 °C leads to the formation of a single brookite. The TiO<sub>2</sub> polymorph heterophase synthesized by Castrejón-Sánchez et al. [214] which can control the anatase/rutile ratio. Initially, anatase-amorphous TiO<sub>2</sub> powder was synthesized by the sol–gel method. Then, annealing was carried out with a time ranging from 35 to 200 min at 475 °C. By adjusting the annealing duration, it is feasible to manage the anatase/rutile ratio in nanostructured TiO<sub>2</sub> powders from pure anatase to

rutile. Figure 10 shows the sol–gel synthesis process with  $\text{Ti}(\text{O}i\text{Bu})_4$  precursor using isobutyl alcohol and the addition of  $\text{HNO}_3$  to produce anatase/rutile heterophase.

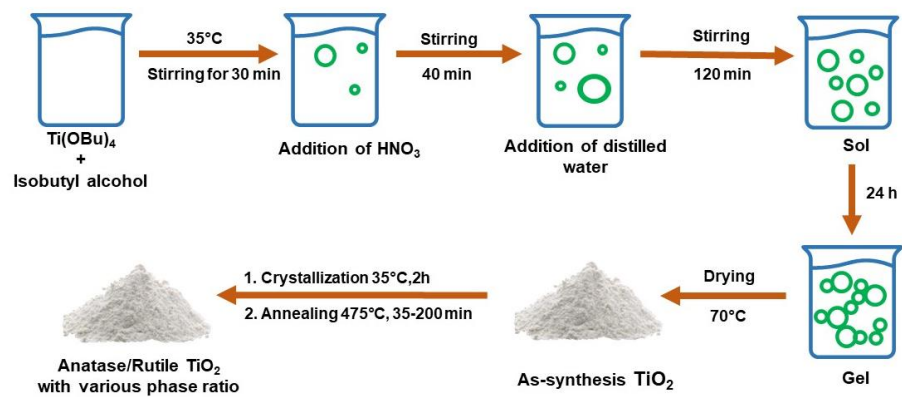


**Figure 10.** Schematic of sol–gel method to produce anatase/rutile heterophase.

### 3.3.2. Hydrothermal Method

The hydrothermal process has strengths over other procedures, including excellent purity and crystallinity in the synthesized materials. Additionally, this technique yields a homogenous particle size distribution with a performance of more than 90% [215–219]. In the hydrothermal method, the trigger for the appearance of the rutile phase is pH [220], using the precursor [221], and using certain solvents [222]. The addition of additives can also trigger the appearance of the rutile phase in  $\text{TiO}_2$ , such as adding urea as a nitrogen source in  $g\text{-C}_3\text{N}_4/\text{TiO}_2$  [222], tartaric acid ( $\text{C}_4\text{H}_6\text{O}_6$ ) [223], or adding metal impurities [224–226].

In a study conducted by Wang et al. [227], mixed-phase  $\text{TiO}_2$  was prepared by the hydrothermal method from  $\text{TiOSO}_4$  and peroxide titanic acid (PTA). The findings demonstrated that anatase and rutile phases made up the mixed-phase  $\text{TiO}_2$  powder, and that the PTA sol was crucial to the development of the rutile core. By adjusting the quantity of PTA sol utilized in the synthesis process, it is simple to control the amount of rutile in the  $\text{TiO}_2$  mixed phase between 0% and 70.5%. Figure 11 shows the hydrothermal method with addition of PTA to produce anatase/rutile heterophase. Meanwhile, in a study by Yang et al. [228], rutile, anatase, and brookite  $\text{TiO}_2$  nanorods were obtained by the hydrothermal method using PTA with different pH values. Rutile forms at pH values below 10, but anatase  $\text{TiO}_2$  can form at pH values over 10. Once the pH is 10, brookite can form.

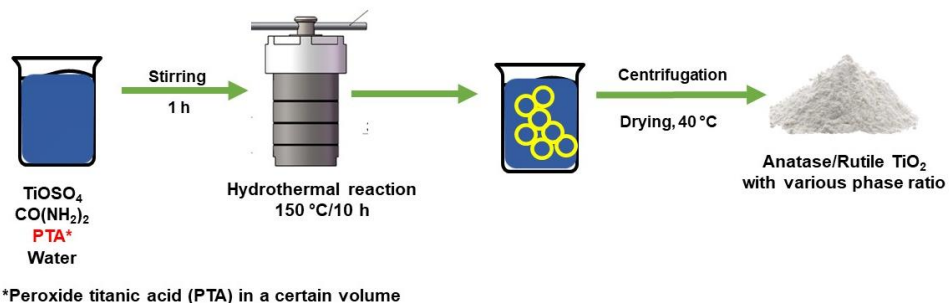


**Figure 11.** Schematic of hydrothermal method to produce anatase/rutile heterophase.

### 3.3.3. Sonochemical Method

Sonochemistry has been widely used to synthesize nano-sized materials [229–233]. Arami et al. [234] synthesized  $\text{TiO}_2$  nanoparticles with an average diameter of about 20 nm via a simple sonochemical method. The results indicated the nanoparticles consisted of a pure rutile phase. Meanwhile, for the mixed phase, anatase/rutile was prepared

by a sonochemical process in which titanium(IV) isopropoxide (TTIP) was used as a precursor. The transformation of the anatase phase to the rutile phase in  $\text{TiO}_2$  powder was initially obtained by calcining the sample at  $600\text{ }^\circ\text{C}$ . The complete rutile phase occurs at the calcination temperature of  $800\text{ }^\circ\text{C}$  [235]. The best photocatalytic activity was demonstrated by an anatase/rutile composite with the proper ratio in a  $\text{TiO}_2$  photocatalyst that was calcined at  $700\text{ }^\circ\text{C}$  as a result of improved charge transfer at the mixed phase junction and reduced electron–hole pair recombination [236]. In addition, anatase/brookite composites have also been synthesized at  $50\text{ }^\circ\text{C}$  using sonochemical methods with similar crystal size and specific surface area, the photocatalytic activity of anatase/brookite for  $\text{CH}_3\text{CHO}$  degradation is 5.4 times higher than in pure anatase. According to the electron energy loss spectrum, the collision of brookite and anatase crystals caused this high activity [237]. Figure 12 shows the sonochemical method with the TTIP precursor using ethanol and water as solvent to produce the anatase/rutile heterophase.

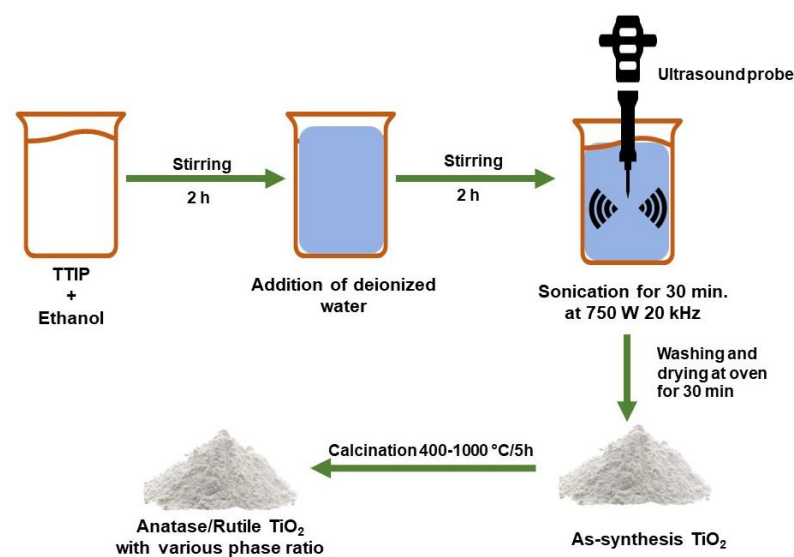


**Figure 12.** Schematic of sonochemical method to produce anatase/rutile heterophase.

### 3.4. Transformation of Polymorph $\text{TiO}_2$

The initial crystalline phase of  $\text{TiO}_2$  that forms during the various processes used to synthesize it is typically anatase. This may be owing to the usual  $\text{TiO}_6$  octahedral's easier organization into a typical anatase structure when compared to rutile from a structural perspective [238]. From a thermodynamic perspective, the faster recrystallization of anatase can be due to the lower surface free energy compared to rutile [137]. However, some studies have been able to form rutile at room temperature conditions. The hydrothermal synthesis approach makes it possible to control the precipitation of rutile while facilitating the direct deposition of  $\text{TiO}_2$  crystals from the liquid phase. Rutile can only be obtained using this technique and high-temperature processing otherwise [239]. As the calcination changes in temperature, the proportions of rutile and anatase will progressively change as well. With higher calcination temperatures, the proportion of the rutile phase increases, which causes the proportion of the anatase phase to diminish [240]. Without any precursor or dopant modification, when making  $\text{TiO}_2$ , the anatase to rutile conversion typically takes place between  $600$  and  $700\text{ }^\circ\text{C}$  [241]. Yuangpho et al. [242] examined the temperature of the anatase–rutile transformation and its impact on the material's physical/chemical characteristics and photocatalytic activity. The photocatalytic activity of  $\text{TiO}_2$  decreases with increasing annealing temperature. These findings suggest that the phase composition influences the photocatalytic activity of  $\text{TiO}_2$  particles.

## 4. Photocatalytic Activity of Heterophase TiO<sub>2</sub>

### 4.1. Biphasic of TiO<sub>2</sub>

#### 4.1.1. Anatase/Rutile

Anatase and rutile are the most common phase of TiO<sub>2</sub> [243]. As a single phase, anatase has better photocatalytic activity than rutile [244]. However, the mixed anatase/rutile phases showed higher photocatalytic activity than single anatase [245]. Rutile is the most stable form compared to the other two forms that are metastable, brookite, and, anatase so at high temperatures it will turn into rutile [246]. It is common to regulate the calcination temperature to produce TiO<sub>2</sub> with a mixture of anatase and rutile phases [247–251]. However, there are also other factors that can be used to control the appearance of these two phases such as the pH and the solvent used [252,253]. Several reports on the formation of mixed phase anatase/rutile structures are summarized in Table 2.

**Table 2.** Various methods for synthesis TiO<sub>2</sub> anatase/rutile.

Precursor	Method	Phase Controller	Application	Ref.
TiO <sub>2</sub> P25	Hydrothermal	Calcination temperature	Water splitting	[63]
TTIP	Hydrothermal	Calcination temperature	Methylene blue degradation	[247]
TTIP	Sol–gel	Calcination temperature	Oxalic acid degradation	[248]
TBOT	Hydrothermal	pH	Hydrogen generation	[252]
TiOSO <sub>4</sub>	Urea precipitation method	Calcination temperature	4-chlorophenol degradation	[250]
TiCl <sub>4</sub>	One step condensing reflux	Solvent	Rhodamine B degradation	[253]
TiCl <sub>3</sub>	Hydrothermal	Calcination temperature	Hydrogen generation	[251]

TiO<sub>2</sub> with anatase/rutile can be used for the production of hydrogen, water splitting, and the degradation of organic pollutants. The factors that influence the increase in anatase/rutile photocatalyst activity are numerous energy-level staggered interfaces between the anatase and rutile, large specific surface area, and an enhancement in bridged hydroxyl functional groups on the surface [253].

Photocatalysis activity and degradation pathways from TiO<sub>2</sub> with mixed phases are dependent on organic substances targeted by photocatalysis [254]. In many cases, increased anatase content tends to result in better TiO<sub>2</sub> photocatalysis activity [255]. When combined with rutile, which is large in size and has high crystallinity, it will be an excellent photocatalytic. This is because degradation is a reaction that requires oxygen and anatase is a good oxygen absorber when compared to rutile. In addition, rutiles that have high crystallinity can also increase intrinsic photocatalysis activity [256]. The synergistic interaction between the anatase (011) and (110) rutile fields, which can also enhance the separation of electron holes and suppress electron and hole recombination, resulting in good photocatalysis activity [257]. Table 3 shows the performance of anatase/rutile photocatalytic degradation for the organic pollutants. Photocatalytic activity against the degradation of organic compounds is carried out by adding photocatalysts to the solution of organic compounds; then, concentration reduction was observed with a UV–vis spectrophotometer [247], or by measuring the conductivity of CO<sub>2</sub> resulting from degradation [248]. For hydrogen generation, the hydrogen formation is measured with gas chromatography (GC) [249].

**Table 3.** Photocatalytic activity of heterophase anatase/rutile.

Pollutant	Optimum Composition (%) *	Dye Concentration	Light Source	Irradiation Time (min)	Efficiency (%)	Ref.
Methylene blue	A 78.5 R 21.5	$1 \times 10^{-5}$ M	UV lamp	20	~94%	[248]
Rhodamine B	A 48.0 R 52.0	4.8 mg/L	300 W Xenon lamp (365 nm)	60	99%	[253]
Methyl orange	A 70.0 R 30.0	20 mg/L	125 W Mercury lamp (365 nm)	40	90.6%	[258]
Methylene blue	A 30.8 R 69.2	$2.92 \times 10^{-5}$ M	175 W UV lamp	90	85.8%	[220]
Crystal violet	A 81.6 R 18.4	100 ppm	UV lamp (365 nm)	300	92.65%	[259]
Methylene blue	A 81.6 R 18.4	100 ppm	UV lamp (365 nm)	300	94.77%	[259]

\* A: Anatase, R: Rutile.

According to Ding et al. [63] the photocatalytic activity for the production of hydrogen ( $H_2$ ) and oxygen ( $O_2$ ) from pure water was significantly increased by the anatase/rutile synthesized using the hydrothermal/calcination method. It proves that rutile/anatase performed significantly better than pure rutile and pure anatase. In another study, anatase/rutile nanoparticles were modified with oxygen vacancies ( $TiO_{2-x}$ ). This heterophase  $TiO_{2-x}$  nanoparticles exhibit superior photocatalytic activity for converting  $CO_2$  to methane and can accelerate electron-hole separation [260].

#### 4.1.2. Anatase/Brookite

Among the three main crystallographic forms of  $TiO_2$ , metastable brookite has received the least amount of research due to the difficulties with its synthesis in a pure form [261]. However, the development of several successful methods such as hydrothermal and sol-gel methods, pure brookite now exists. For photocatalytic activity, pure anatase exhibits a higher activity compared to other phases because the indirect band gap can exhibit lower recombination rates due to the longer lifetimes for photo-excited electrons and holes [70]. However, phase mixtures of various polymorphs are known to have synergistic effects and exhibit improved photocatalytic activity [56]. Compared to anatase/rutile, mixed-phase titania containing brookite has received less attention [262]. Table 4 summarizes a few studies on the preparation of mixed-phase  $TiO_2$  nanostructures with a tuned ratio of brookite in the titania mixtures. Meanwhile, Table 5 shows the performance of anatase/brookite photocatalytic degradation for the organic pollutants.

**Table 4.** Various methods for synthesis  $TiO_2$  anatase/brookite.

Precursor	Method	Additive	Application	Ref.
TALH	Hydrothermal	Urea	Hydrogen production and dichloroacetic acid (DCA) degradation	[263]
$TiCl_3$	Hydrothermal	Tartaric acid	Rhodamine B degradation	[264]
$TiCl_3$	Hydrothermal	NaCl and $NH_4OH$	Rhodamine B degradation	[265]
$TiS_2$	Hydrothermal	NaOH	Hydrogen generation	[266]
$Ti_2(SO_4)_3$	Hydrothermal	Glycine with $NH_4OH$ or NaOH	Cylindrospermopsin degradation	[267]
TTIP	Sol-gel	$HNO_3$	Methylene blue degradation	[268]
TTIP	Microwave assisted sol-gel	HCl and $CH_3COOH$	-	[269]
TTIP	Ultrasonic-assisted sol-gel	$HNO_3$ and $CH_3COOH$	Methylene blue degradation	[270]
TTIP	Sol-gel complex	hydroxycarboxylic acids	Hydrogen generation	[271]
$Ti(Opr)_4$	Sol-gel complex	Lactic acid	Hydrogen generation	[272]
$Ti_2(SO_4)_3$	Hydrothermal	Glycine with $NH_4OH$ or NaOH	Diclofenac degradation	[273]

**Table 5.** Photocatalytic activity of heterophase anatase/brookite.

Pollutant	Optimum Composition (%) *	Photocatalyst Loading	Dye Concentration	Light Source	Irradiation Time (min)	Efficiency (%)	Ref.
Rhodamine B	A 78.7 B 21.3	-	20 mg/L	300 W Hg lamp (365 nm)	120	98	[264]
Rhodamine B	A 46.6 B 53.4	-	20 mg/L	300 W Hg lamp (365 nm)	100	95	[265]
Methylene blue	A 80.0 B 20.0	0.6 g/L	32 mg/L	100 W mercury lamp	70	98	[268]
Methylene blue	A 79.0 B 21.0	1 g/L	5 mg/L	100 W UV lamp (365 nm)	240	60	[270]
Cylindrospermopsin (CYN)	A 61.8 B 38.2	0.25 g/L	$1 \times 10^{-6}$ M	15 W florescence lamp (310–720 nm)	15	100	[267]
Diclofenac (DCF)	A 61.8 B 38.2	1 g/L	10 mg/L	UV-A irradiation	120	100	[262]

\* A: Anatase, B: Brookite.

Anatase/brookite is successfully produced by hydrothermal method using titanium bis(ammonium lactate) dihydroxide (TALH) in the presence of high concentrations of urea ( $\geq 6.0$  M) as an in situ OH<sup>−</sup> source. Lower urea concentrations lead to the formation of anatase/brookite mixtures. According to the results, pure anatase is less effective for hydrogen evolution than mixtures of anatase/brookite or pure brookite. On the other hand, pure brookite and mixtures of anatase and brookite show lower photocatalytic activity compared to pure anatase for the photocatalytic degradation of dichloroacetic acid (DCA) that performed at pH 3 [263]. However, TALH is neither affordable nor environmentally friendly (causing a release of ammonia) [262]. Another research work used titanium trichloride (TiCl<sub>3</sub>) as the titanium source, which can be easily manipulated, and uses tartaric acid (C<sub>4</sub>H<sub>6</sub>O<sub>6</sub>), which is low-cost and safe [265]. The as-prepared TiO<sub>2</sub> that consisted of 78.7% anatase and 21.3% brookite showed the highest photocatalytic activity for Rhodamine B degradation, which was 1.2 times greater than commercial P25. A UV–Vis spectrometer was used to measure the maximum absorbance in order to determine the concentration of Rhodamine B. Meanwhile, anatase/brookite synthesized by an alkaline hydrothermal treatment of TiCl<sub>3</sub> by adjusting the NaCl concentration and NH<sub>4</sub>OH/H<sub>2</sub>O volume ratio showed that the product containing 53.4% brookite and 46.6% anatase shows the highest photocatalytic activity for degradation Rhodamine B, which is higher than pure phase [266]. For synthesized via a simple hydrothermal method with titanium sulfide (TiS<sub>2</sub>) as the precursors in sodium hydroxide solutions showed anatase/brookite TiO<sub>2</sub> is 2.2 times more active—when measured by the H<sub>2</sub> yield per unit area of the photocatalyst surface—than commercial P25 [267]. Another research work using titanium(III) sulfate (Ti<sub>2</sub>(SO<sub>4</sub>)<sub>3</sub>) in the presence of glycine through hydrothermal treatment shows that a sample containing 38.2% brookite and 61.8% anatase exhibited the highest efficiency for the removal cylindrospermopsin (CYN) and diclofenac than pure anatase, pure brookite, and commercial P25. The concentration of CYN was analyzed by high-performance liquid chromatography with a photodiode-array detector (PDA). Meanwhile, diclofenac concentration is measured by the UV–vis spectrophotometer [262,267].

TiO<sub>2</sub> nanoparticles with anatase/brookite were also synthesized using a modified sol–gel method at low temperatures [268]. The mixture obtained at pH 2 and calcined at 200 °C had the highest activity for methylene blue degradation that measured by UV–Vis spectroscopy at 660 nm compared to commercial P25. The modified conventional sol–gel method is using the microwave-assisted sol–gel technique [269]. The phase transformation of TiO<sub>2</sub> was investigated by hydrochloric and acetic acid. Three titania polymorphs were found when hydrochloric acid was used as a catalyst. On the other hand, a single anatase phase was obtained when acetic acid was added after only 15 min of reaction time. The ultrasonic-assisted sol–gel method [270], which used weak and strong acids, demonstrated a significant effect on their morphology, size, crystallinity, and photocatalytic performance.

The photocatalytic activity showed that anatase and rutile phases with a high proportion of anatase (69:31 and 93:7, respectively), had the highest photoactivity for the degradation of MB compared with anatase/brookite (70:30).

According to Cihlar et al. [271], anatase/brookite is produced using the sol–gel complex method. This method consists of sol–gel, hydrothermal, and solid-state reactions that used titanium tetraisopropoxide (TTIP) as the precursor and the complex-forming (chelate-forming) substances used were glycine, EDTA, acetylacetone, and hydroxycarboxylic acids (lactic acid (LA), citric acid (CA), and tartaric acid (TA)) and their salts. These materials use to produce hydrogen by photocatalysis. The results show that anatase/brookite nanoparticles with 36% brookite, which were made using lactic acid, catalyzed the maximum rate of H<sub>2</sub> evolution. The presence of anatase particles made using acetylacetone was found to have the lowest rate of H<sub>2</sub> evolution. Another research work investigated the phase composition of TiO<sub>2</sub> using lactic acid/Ti molar ratio ranging from 0.02 to 3.0 ratio via sol–gel complex synthesis [272]. Anatase/brookite was formed at low LA/Ti molar ratios, followed by anatase/brookite/rutile particles at average molar ratios, and pure anatase at high molar ratios. Anatase/brookite nanoparticles made at LA/Ti molar ratios between 0.03 and 0.1 showed the highest photocatalytic activity in the production of hydrogen by water splitting. Table 6 shows the performance of heterophase TiO<sub>2</sub> for hydrogen production.

**Table 6.** Photocatalytic activity of heterophase TiO<sub>2</sub> for hydrogen production.

Optimum Composition (%) *	Amount of Catalyst	Light Source	H <sub>2</sub> Evolution Rate	Ref.
A 73.5 R 26.5	20 mg/100 mL	300 W Xe lamp	584 μmol g <sup>-1</sup> h <sup>-1</sup>	[63]
A 12.0 R 88.0	20 mg/80 mL	350 W Xe lamp	74,400 μmol g <sup>-1</sup> h <sup>-1</sup>	[252]
A 72.0 B 28.0	37.5 mg/75 mL	1000 W Xe lamp	4267 μmol g <sup>-1</sup> h <sup>-1</sup>	[263]
A 88.4 B 11.6	45 mg/100 mL	800 W Xe–Hg lamp	~3500 μmol g <sup>-1</sup> h <sup>-1</sup>	[266]
A 74.0 B 36.0	20 mg/100 mL	450 W Xe lamp	101.4 μmol g <sup>-1</sup> min <sup>-1</sup>	[271]
A 54.0 B 46.0	20 mg/100 mL	450 W Xe lamp	101.4 μmol g <sup>-1</sup> min <sup>-1</sup>	[272]

\* A: anatase, R: rutile, B: brookite.

#### 4.1.3. Rutile/Brookite

Rutile/brookite as a photocatalyst was reported in 2008 by Di Paola et al. [273]. The sample was synthesized by thermohydrolysis of TiCl<sub>4</sub> in HCl or NaCl aqueous solutions. Rutile mixtures were obtained depending on the acidity of the medium. The photocatalytic activity was evaluated by 4-nitrophenol degradation and quantitative determination was performed by measuring its absorption at 315 nm with a spectrophotometer UV. The highest photocatalytic activity for 4-nitrophenol degradation corresponded to the powders consisting of heterophase, compared to the pure phase [274].

Another way to synthesize a controlled rutile/brookite is by the hydrothermal method. This method uses titanium tetrachloride as a titanium source and triethylamine as a “regulating reagent” to adjust the ratio of brookite to rutile. The research found that the TiO<sub>2</sub> sample with the highest photocatalytic activity for RhB degradation was obtained in a solution of 3 mL triethylamine and 10 mL water and contained 38% brookite and 62% rutile [275].

In another study, brookite/rutile was obtained using the solvothermal method. The morphology and structure of the samples were greatly changed by varying the ratio of  $\text{TiCl}_4$  to  $t\text{-BuOH}$  precursors. The phenol degradation measured by HPLC system showed that the highest photocatalytic activity was obtained from a composition of 72% brookite and 28% rutile. The highest phenol degradation activity was obtained from a composition of 72% brookite and 28% rutile. This indicates that the biphasic structure of brookite/rutile with optimized phase proportions is responsible for the efficient synergy effect [276,277].

#### 4.1.4. Biphasic of $\text{TiO}_2$ (B)

$\text{TiO}_2$  (B) is a less stable phase of  $\text{TiO}_2$  than anatase and rutile [114]. When compared to anatase, rutile, and brookite,  $\text{TiO}_2$  (B) is the least dense polymorph of  $\text{TiO}_2$  [278].  $\text{TiO}_2$  (B) is suitable for use as a place of Li intercalation because it has a structure that is relatively open, with free space and continuous channels [115]. The synthetic  $\text{TiO}_2$  (B) nanowire-based electrode exhibited unique electronic properties, e.g., favourable charge-transfer ability, negative-shifted appeared flat-band potential, the existence of abundant surface states or oxygen vacancies, and high-level donor density [279,280]. There is an alternative synthesis of  $\text{TiO}_2$  (B), through the formation of a titanium complex obtained from the reaction between titanium metal powder and  $\text{H}_2\text{O}_2$ ,  $\text{NH}_3$ , and glycolic acid which produces a yellowish gel. The resulting gel is then added to  $\text{H}_2\text{SO}_4$  to change the pH and put into the autoclave for hydrothermal treatment [173]. According to research by Wang et al. [73], the right quantity of HF could prevent the phase transition of  $\text{TiO}_2$  (B) to anatase. The mechanism of this phase transformation occurs because the F anion adsorbed on the surface of  $\text{TiO}_2$  (B) can efficiently reduce the surface energy from  $0.63 \text{ J/m}^2$  for a clean surface to  $-0.22 \text{ J/m}^2$  for the surface adsorbed on F anion. Several methods for synthesizing  $\text{TiO}_2$  (B) are shown in Table 7.

**Table 7.** Various methods for synthesis  $\text{TiO}_2$  (B).

Precursor	Method	Additive	Application	Ref.
Titanium metal powder	Post-synthetic Hydrothermal crystal growth	$\text{H}_2\text{SO}_4$	-	[281]
Titanium metal powder	Hydrothermal	$\text{H}_2\text{SO}_4$	-	[282]
$\text{TiCl}_4$	Solvothermal	-	Lithium-ion batteries	[173]
$\text{TiO}_2$ P25	Hydrothermal	-	DSSC	[278]
$\text{TiO}_2$ P25	Hydrothermal	-	Humidity sensors	[279]
TTIP	Surfactant-assisted nonaqueous sol-gel route	Oleic acid	Lithium ion-batteries	[283]

However,  $\text{TiO}_2$  (B), as a photocatalyst composited with another  $\text{TiO}_2$  polymorph, was performed by Li et al. [67]. The biphasic structure of  $\text{TiO}_2$  was synthesized from  $\text{K}_2\text{Ti}_2\text{O}_5$  through ion exchange and calcination. The nanofiber of core-shell crystal structure had a thin  $\text{TiO}_2$  (B) shell and an anatase core. The core-shell anatase/ $\text{TiO}_2$  (B) nanofiber showed increased photocatalytic activity in iodine oxidation reactions, with a reaction increase of 20–50% compared to single crystal anatase nanofiber or single crystal  $\text{TiO}_2$  (B). The same m was also conducted by Yang et al. [61], by synthesizing core-shell  $\text{TiO}_2$  (B)/anatase. A number of characteristics of this unusual structure improve the photocatalytic activity against the degradation of sulforhodamine B when exposed to UV light.

The advantage of having a biphasic structure of  $\text{TiO}_2$  (B)/anatase is that  $\text{TiO}_2$  (B) and anatase will form a heterojunction; the photogenerated electrons and holes can be transferred to the anatase phase and  $\text{TiO}_2$  (B) phase, respectively (Figure 13), thereby reducing recombination [195,284]. In the study of Mikrut et al. [285],  $\text{TiO}_2$  (B)/anatase was synthesized in the form of nanobelts. Similar to the anatase/rutile composite, a synergistic effect of

the presence of the two phases was observed for TiO<sub>2</sub> (B)/anatase (2:98). It is well known that TiO<sub>2</sub> (B) is regarded as an optimized photocatalyst component for oxidation reactions involving hydroxyl radicals rather than promoting hydrogen evolution reactions.

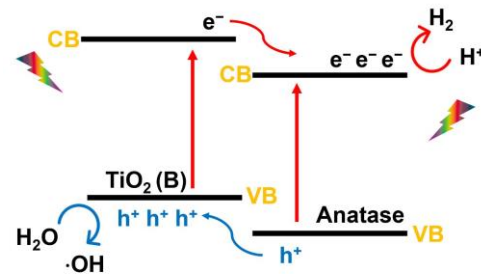


**Figure 13.** Schematic diagram illustrating the charge transfer across the TiO<sub>2</sub> (B)/anatase heterophase junction.

Zhu et al. [286] reported another TiO<sub>2</sub> (B) heterophase. In their research, the disintegration of TiO<sub>2</sub> (B)/rutile used hydrothermal and calcination methods. The two phases are connected by an angle division at the phase interface (Figure 14). Electrons and holes are effectively separated across the phase interface as a result of the different conduction band and valence band positions between the two phases. The best results as photocatalysis were obtained at a TiO<sub>2</sub> (B)/rutile ratio of 2/1, indicating the highest photocurrent and the best H<sub>2</sub> evolution performance.

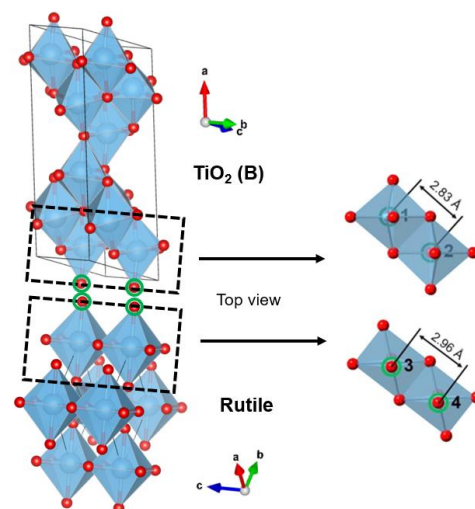


**Figure 14.** Possible connection model of the mixed phase at the phase interface.

#### 4.2. Triphase of TiO<sub>2</sub>

Numerous studies have been conducted to improve the activity of TiO<sub>2</sub>, but the two most significant findings are increasing the specific surface area and using the mixed phase [287]. The triphase of polymorph TiO<sub>2</sub> shows a significant increase in photocatalytic activity compared to the pure and biphasic phases [71]. Allen et al. [288] reported the effect of thermal treatment of heterophase polymorph TiO<sub>2</sub> prepared by hydrolyzing titanium tetraisopropoxide at room temperature, dried at 382 K, and calcined at different temperatures for 1 h up to 1172 K. The results demonstrate that a mixture of brookite and anatase phases were seen up to 772 K, while a mixture of all three phases (anatase, brookite, and rutile) was present at 872 K, and a rutile-only phase was present at 1097 K and above.

Fischer et al. [70], synthesized a mixture of TiO<sub>2</sub> phases (anatase, rutile, and brookite) on a polyethersulfone (PES) membrane via low-temperature dissolution-precipitation. In order to achieve that, the concentration of titanium precursor (titanium(IV) isopropoxide)

was held constant while the amounts of hydrochloric acid and reaction temperature were adjusted to range from 0.1 to 1 M and 25 to 130 °C, respectively. The result showed that the best degradation rate of methylene blue were measured via microplate reader at a wavelength of  $\lambda = 660$  nm, showing the highest activity that was obtained by 79% anatase and 21% brookite. Meanwhile, the recovery test showed that anatase, brookite, and rutile samples (70, 26, and 4%, respectively) did not degrade and completely recovered their photocatalytic abilities after at least nine additional cycles.

In a different study by Kaplan et al. [289], the formation of TiO<sub>2</sub> that consists of anatase (43%), rutile (24%), and brookite (33%) was obtained by synthesizing TiO<sub>2</sub> mixed phase using the sol–gel method and then hydrothermally treating it at a mild temperature (175 °C, 24 h). It was discovered that the photocatalytic activity of TiO<sub>2</sub> nanocomposite successfully converted nearly 60% of the pollutant bisphenol into CO<sub>2</sub> in H<sub>2</sub>O after being irradiated by UV light for 60 min. In contrast, only a lower level of mineralization was attained by the TiO<sub>2</sub> P25 Degussa benchmark catalyst. This is due to a significantly reduced resistance to the accumulation of carbonaceous deposits on the catalyst surface.

## 5. Conclusions

This review summarizes most of the papers on TiO<sub>2</sub> polymorphs (anatase, rutile, brookite, and TiO<sub>2</sub> (B)), pure-phase TiO<sub>2</sub> photocatalytic mechanisms, mixed phase, synthesis methods, and photocatalytic activities. This paper explains how to obtain pure phases from various TiO<sub>2</sub> polymorphs and examples of their application in photocatalysis. In many cases, anatase has better activity than rutile and brookite. However, several studies have shown that rutile and brookite may have better activity in certain cases. Even thus, one-phase TiO<sub>2</sub> has some drawbacks, such as high recombination and low specific surface area. TiO<sub>2</sub> mixed phase shows better activity than the pure phase. This is due to good charge separation due to the formation of junctions around the interface. In addition, the synthesis methods that are often used to prepare mixed-phase TiO<sub>2</sub> are sol–gel, hydrothermal, and sonochemical methods. Although the phase controller is usually the annealing temperature for anatase/rutile, in the hydrothermal method, additives are usually used as phase controllers.

Photocatalytic activity shows that anatase/rutile has much better activity than pure anatase or rutile. In addition, development continues to see the activity of other heterophases, such as anatase/brookite, rutile/brookite, and the heterophase TiO<sub>2</sub> (B). However, in the case of brookite and TiO<sub>2</sub> (B), the synthesis tends to be more difficult, these heterophase results show good photocatalytic activity. In addition, the triphase of polymorph TiO<sub>2</sub> showed good photocatalytic activities for organic pollutants degradation. However, further studies to determine the exact number of compositions for each polymorph for the best activity in triphase TiO<sub>2</sub> have not yet been investigated. In conclusion, further investigations are recommended to explore an easy method to synthesize TiO<sub>2</sub> polymorphs with a high specific surface area and investigate the best composition of each TiO<sub>2</sub> polymorph for photocatalytic activity, especially for triphase.

**Author Contributions:** D.R.E., S., S.H., T.T., N.K. and I.R. conceptualized the article and supervised the overall work; M.D.P., L.K.S. and G.A.N.S. wrote the original article; M.D.P. and L.K.S. visualized the figures and illustrations. All authors contributed to the writing and revising of the manuscript. All authors have read and agreed to the published version of the manuscript.

**Funding:** This research was funded by The Riset Data Pustaka dan Daring (RDPD) (ID: 2203/UN6.3.1/PT.00/2022) and Academic Leadership Grant (ALG) Prof. Iman Rahayu, Universitas Padjadjaran (ID: 2203/UN6.3.1/PT.00/2022) for supporting financially.

**Institutional Review Board Statement:** Not applicable.

**Informed Consent Statement:** Not applicable.

**Data Availability Statement:** The study did not report any data.

**Conflicts of Interest:** The authors declare no conflict of interest.

## References

- Haider, A.J.; Jameel, Z.N.; Al-Hussaini, I.H. Review on: Titanium dioxide applications. *Energy Procedia* **2019**, *157*, 17–29. [[CrossRef](#)]
- Eddy, D.R.; Ishmah, S.N.; Permana, M.D.; Firdaus, M.L. Synthesis of titanium dioxide/silicon dioxide from beach sand as photocatalyst for Cr and Pb remediation. *Catalysts* **2020**, *10*, 1248. [[CrossRef](#)]
- Chen, X.; Mao, S.S. Titanium dioxide nanomaterials: Synthesis, properties, modifications, and applications. *Chem. Rev.* **2007**, *107*, 2891–2959. [[CrossRef](#)]
- Glassford, K.M.; Chelikowsky, J.R. Structural and electronic properties of titanium dioxide. *Phys. Rev. B* **1992**, *46*, 1284–1298. [[CrossRef](#)]
- Grant, F.A. Properties of rutile (titanium dioxide). *Rev. Mod. Phys.* **1959**, *31*, 646–674. [[CrossRef](#)]
- Breckenridge, R.G.; Hosler, W.R. Electrical properties of titanium dioxide semiconductors. *Phys. Rev.* **1953**, *91*, 793–802. [[CrossRef](#)]
- Chen, D.; Cheng, Y.; Zhou, N.; Chen, P.; Wang, Y.; Li, K.; Huo, S.; Cheng, P.; Peng, P.; Zhang, R.; et al. Photocatalytic degradation of organic pollutants using TiO<sub>2</sub>-based photocatalysts: A review. *J. Clean. Prod.* **2020**, *268*, 121725. [[CrossRef](#)]
- Barbosa, J.S.; Neto, D.M.A.; Freire, R.M.; Rocha, J.S.; Fechine, L.M.U.D.; Denardin, J.C.; Valentini, A.; de Araújo, T.G.; Mazzetto, S.E.; Fechine, P.B.A. Ultrafast sonochemistry-based approach to coat TiO<sub>2</sub> commercial particles for sunscreen formulation. *Ultrason. Sonochem.* **2018**, *48*, 340–348. [[CrossRef](#)]
- Jafari, S.; Mahyad, B.; Hashemzadeh, H.; Janfaza, S.; Gholikhani, T.; Tayebi, L. Biomedical Applications of TiO<sub>2</sub> Nanostructures: Recent Advances. *Int. J. Nanomed.* **2020**, *15*, 3447–3470. [[CrossRef](#)]
- Gázquez, M.J.; Bolívar, J.P.; García-Tenorio, R.; Vaca, F. A review of the production cycle of titanium dioxide pigment. *Mater. Sci. Appl.* **2014**, *2*, 441–458. [[CrossRef](#)]
- Day, R.E. The role of titanium dioxide pigments in the degradation and tabilization of polymers in the plastics industry. *Polym. Degrad. Stab.* **1990**, *29*, 73–92. [[CrossRef](#)]
- Middlemas, S.; Fang, Z.Z.; Fan, P. A new method for production of titanium dioxide pigment. *Hydrometallurgy* **2013**, *131*, 107–113. [[CrossRef](#)]
- Gesenhues, U. Calcination of metatitanic acid to titanium dioxide white pigments. *Chem. Eng. Technol.* **2001**, *24*, 685–694. [[CrossRef](#)]
- Yang, B.; Wang, M.; Hu, X.; Zhou, T.; Zang, Z. Highly efficient semitransparent CsPbI<sub>2</sub>Br<sub>2</sub> perovskite solar cells via low-temperature processed In<sub>2</sub>S<sub>3</sub> as electron-transport-layer. *Nano Energy* **2019**, *57*, 718–727. [[CrossRef](#)]
- Tan, X.; Liu, X.; Liu, Z.; Sun, B.; Li, J.; Xi, S.; Shi, T.; Tang, Z.; Liao, G. Enhancing the optical, morphological and electronic properties of the solution-processed CsPbI<sub>2</sub>Br<sub>2</sub> films by Li doping for efficient carbon-based perovskite solar cells. *Appl. Surf. Sci.* **2020**, *499*, 143990. [[CrossRef](#)]
- Islam Molla, M.A.; Tateishi, I.; Furukawa, M.; Katsumata, H.; Suzuki, T.; Kaneco, S. Evaluation of Reaction Mechanism for Photocatalytic Degradation of Dye with Self-Sensitized TiO<sub>2</sub> under Visible Light Irradiation. *Open J. Inorg. Non met. Mater.* **2017**, *7*, 1–7.
- Rabajczyk, A.; Zielecka, M.; Klapsa, W.; Dziechciarz, A. Self-cleaning coatings and surfaces of modern building materials for the removal of some air pollutants. *Materials* **2021**, *14*, 2161. [[CrossRef](#)]
- Roy, P.; Kim, D.; Lee, K.; Schmuki, P. TiO<sub>2</sub> nanotubes and their application in dye-sensitized solar cells. *Nanoscale* **2010**, *2*, 45–59. [[CrossRef](#)]
- Preethi, V.; Kanmani, S. Photocatalytic hydrogen production. *Mater. Sci. Semicond. Process.* **2013**, *16*, 561–575. [[CrossRef](#)]
- Teets, T.S.; Nocera, D.G. Photocatalytic hydrogen production. *ChemComm.* **2011**, *47*, 9268–9274. [[CrossRef](#)]
- Zhu, J.; Zäch, M. Nanostructured materials for photocatalytic hydrogen production. *Curr. Opin. Colloid Interface Sci.* **2009**, *4*, 260–269. [[CrossRef](#)]
- Du, H.; Liu, Y.N.; Shen, C.C.; Xu, A.W. Nanoheterostructured photocatalysts for improving photocatalytic hydrogen production. *Chinese J. Catal.* **2017**, *38*, 1295–1306. [[CrossRef](#)]
- Chatterjee, D.; Dasgupta, S. Visible light induced photocatalytic degradation of organic pollutants. *J. Photochem. Photobiol. C Photochem. Rev.* **2005**, *6*, 186–205. [[CrossRef](#)]
- Shayegan, Z.; Lee, C.S.; Haghighat, F. TiO<sub>2</sub> photocatalyst for removal of volatile organic compounds in gas phase—A review. *Chem. Eng. J.* **2018**, *334*, 2408–2439. [[CrossRef](#)]
- Umar, M.; Aziz, H.A. Photocatalytic degradation of organic pollutants in water. In *Organic Pollutants-Monitoring, Risk, and Treatment*; Rashed, M.N., Ed.; IntechOpen: London, UK, 2013; Volume 8, pp. 196–197.
- Dong, H.; Zeng, G.; Tang, L.; Fan, C.; Zhang, C.; He, X.; He, Y. An overview on limitations of TiO<sub>2</sub>-based particles for photocatalytic degradation of organic pollutants and the corresponding countermeasures. *Water Res.* **2015**, *79*, 128–146. [[CrossRef](#)]
- Paumo, H.K.; Dalhatou, S.; Katata-Seru, L.M.; Kamdem, B.P.; Tijani, J.O.; Vishwanathan, V.; Kane, A.; Bahadur, I. TiO<sub>2</sub> assisted photocatalysts for degradation of emerging organic pollutants in water and wastewater. *J. Mol. Liq.* **2021**, *331*, 115458. [[CrossRef](#)]
- Ameta, R.; Benjamin, S.; Ameta, A.; Ameta, S.C. Photocatalytic degradation of organic pollutants: A review. *Mater. Sci. Forum* **2013**, *734*, 247–272. [[CrossRef](#)]
- Wang, C.C.; Du, X.D.; Li, J.; Guo, X.X.; Wang, P.; Zhang, J. Photocatalytic Cr (VI) reduction in metal-organic frameworks: A mini-review. *Appl. Catal. B* **2016**, *193*, 198–216. [[CrossRef](#)]

30. Kumar, A.; Choudhary, P.; Kumar, A.; Camargo, P.H.; Krishnan, V. Recent advances in plasmonic photocatalysis based on TiO<sub>2</sub> and noble metal nanoparticles for energy conversion, environmental remediation, and organic synthesis. *Small* **2022**, *18*, 2101638. [[CrossRef](#)]
31. Lin, Z.; Zheng, Y.; Deng, F.; Luo, X.; Zou, J.; Shao, P.; Zhang, S.; Tang, H. Target-directed design of dual-functional Z-scheme AgIn<sub>5</sub>S<sub>8</sub>/SnS<sub>2</sub> heterojunction for Pb (II) capture and photocatalytic reduction of Cr (VI): Performance and mechanism insight. *Sep. Purif. Technol.* **2021**, *277*, 119430. [[CrossRef](#)]
32. Hubbard, J.S.; Hardy, J.P.; Voecks, G.E.; Golub, E.E. Photocatalytic synthesis of organic compounds from CO and water: Involvement of surfaces in the formation and stabilization of products. *J. Mol. Evol.* **1973**, *2*, 149–166. [[CrossRef](#)]
33. Lima, M.J.; Silva, A.M.; Silva, C.G.; Faria, J.L.; Reis, N.M. Selective photocatalytic synthesis of benzaldehyde in microcapillaries with immobilized carbon nitride. *Chem. Eng. J.* **2022**, *430*, 132643. [[CrossRef](#)]
34. Luo, J.; Wang, M.; Chen, L.; Shi, J. Efficient benzaldehyde photosynthesis coupling photocatalytic hydrogen evolution. *J. Energy Chem.* **2022**, *66*, 52–60. [[CrossRef](#)]
35. Lima, M.J.; Tavares, P.B.; Silva, A.M.; Silva, C.G.; Faria, J.L. Selective photocatalytic oxidation of benzyl alcohol to benzaldehyde by using metal-loaded g-C<sub>3</sub>N<sub>4</sub> photocatalysts. *Catal. Today* **2017**, *287*, 70–77. [[CrossRef](#)]
36. Chen, J.; Qiu, F.; Xu, W.; Cao, S.; Zhu, H. Recent progress in enhancing photocatalytic efficiency of TiO<sub>2</sub>-based materials. *Appl. Catal. A Gen.* **2015**, *495*, 131–140. [[CrossRef](#)]
37. Dong, P.; Hou, G.; Xi, X.; Shao, R.; Dong, F. WO<sub>3</sub>-based photocatalysts: Morphology control, activity enhancement and multifunctional applications. *Environ. Sci. Nano* **2017**, *4*, 539–557. [[CrossRef](#)]
38. Zhong, Y.; Wang, J.; Zhang, R.; Wei, W.; Wang, H.; Lü, X.; Bai, F.; Wu, H.; Haddad, R.; Fan, H. Morphology-controlled self-assembly and synthesis of photocatalytic nanocrystals. *Nano Lett.* **2014**, *14*, 7175–7179. [[CrossRef](#)]
39. Li, X.; Zheng, W.; He, G.; Zhao, R.; Liu, D. Morphology control of TiO<sub>2</sub> nanoparticle in microemulsion and its photocatalytic property. *ACS Sustain. Chem. Eng.* **2014**, *2*, 288–295. [[CrossRef](#)]
40. Rauf, M.A.; Meetani, M.A.; Hisaindee, S. An overview on the photocatalytic degradation of azo dyes in the presence of TiO<sub>2</sub> doped with selective transition metals. *Desalination* **2011**, *276*, 13–27. [[CrossRef](#)]
41. Kumaravel, V.; Mathew, S.; Bartlett, J.; Pillai, S.C. Photocatalytic hydrogen production using metal doped TiO<sub>2</sub>: A review of recent advances. *Appl. Catal. B* **2019**, *244*, 1021–1064. [[CrossRef](#)]
42. Nah, Y.C.; Paramasivam, I.; Schmuki, P. Doped TiO<sub>2</sub> and TiO<sub>2</sub> nanotubes: Synthesis and applications. *ChemPhysChem* **2010**, *11*, 2698–2713. [[CrossRef](#)]
43. Woan, K.; Pyrgiotakis, G.; Sigmund, W. Photocatalytic carbon-nanotube–TiO<sub>2</sub> composites. *Adv. Mater.* **2009**, *21*, 2233–2239. [[CrossRef](#)]
44. Tang, B.; Chen, H.; Peng, H.; Wang, Z.; Huang, W. Graphene modified TiO<sub>2</sub> composite photocatalysts: Mechanism, progress and perspective. *Nanomaterials* **2018**, *8*, 105. [[CrossRef](#)]
45. He, J.; Kumar, A.; Khan, M.; Lo, I.M. Critical review of photocatalytic disinfection of bacteria: From noble metals-and carbon nanomaterials-TiO<sub>2</sub> composites to challenges of water characteristics and strategic solutions. *Sci. Total Environ.* **2021**, *758*, 143953. [[CrossRef](#)]
46. Tekin, D.; Birhan, D.; Kiziltas, H. Thermal, photocatalytic, and antibacterial properties of calcinated nano-TiO<sub>2</sub>/polymer composites. *Mat. Chem. Phys.* **2020**, *251*, 123067. [[CrossRef](#)]
47. Murad, E. Identification of minor amounts of anatase in kaolins by Raman spectroscopy. *Am. Mineral.* **1997**, *82*, 203–206. [[CrossRef](#)]
48. Lu, Y.; Jaeckel, B.; Parkinson, B.A. Preparation and characterization of terraced surfaces of low-index faces of anatase, rutile, and brookite. *Langmuir* **2006**, *22*, 4472–4475. [[CrossRef](#)]
49. Haggerty, J.E.; Schelhas, L.T.; Kitchaev, D.A.; Mangum, J.S.; Garten, L.M.; Sun, W. High-fraction brookite films from amorphous precursors. *Sci. Rep.* **2017**, *7*, 15232. [[CrossRef](#)]
50. Permana, M.D.; Noviyanti, A.R.; Lestari, P.R.; Kumada, N.; Eddy, D.R.; Rahayu, I. The Effect of Organometallic Precursors on TiO<sub>2</sub> Synthesis and Their Photocatalytic Activity on Phenol Degradation. *Kuwait J. Sci.* **2022**, *49*, 1–13.
51. Deo, G.; Turek, A.M.; Wachs, I.E.; Machej, T.; Haber, J.; Das, N.; Eckert, H.; Hirt, A.M. Physical and chemical characterization of surface vanadium oxide supported on titania: Influence of the titania phase (anatase, rutile, brookite and B). *Appl. Catal. A Gen.* **1992**, *91*, 27–42. [[CrossRef](#)]
52. Dacheville, F.; Simons, P.Y.; Roy, R. Pressure-temperature studies of anatase, brookite, rutile and TiO<sub>2</sub>-II. *Am. Mineral.* **1968**, *53*, 1929–1939.
53. Akpan, U.G.; Hameed, B.H. Parameters affecting the photocatalytic degradation of dyes using TiO<sub>2</sub>-based photocatalysts: A review. *J. Hazard. Mater.* **2009**, *170*, 520–529. [[CrossRef](#)]
54. Sun, J.; Gao, L.; Zhang, Q. Synthesizing and comparing the photocatalytic properties of high surface area rutile and anatase titania nanoparticles. *J. Am. Ceram. Soc.* **2003**, *86*, 1677–1682. [[CrossRef](#)]
55. Maver, K.; Arçon, I.; Fanetti, M.; Emin, S.; Valant, M.; Štangar, U.L. Improved photocatalytic activity of anatase-rutile nanocomposites induced by low-temperature sol-gel Sn-modification of TiO<sub>2</sub>. *Catal. Today* **2021**, *361*, 124–129. [[CrossRef](#)]
56. Luttrell, T.; Halpegamage, S.; Tao, J.; Kramer, A.; Sutter, E.; Batzill, M. Why is anatase a better photocatalyst than rutile?-Model studies on epitaxial TiO<sub>2</sub> films. *Sci. Rep.* **2014**, *4*, 1–8. [[CrossRef](#)]

57. Al-Mamun, M.R.; Kader, S.; Islam, M.S.; Khan, M.Z.H. Photocatalytic activity improvement and application of UV-TiO<sub>2</sub> photocatalysis in textile wastewater treatment: A review. *J. Environ. Chem. Eng.* **2019**, *7*, 103248. [[CrossRef](#)]
58. Lee, M.S.; Hong, S.-S.; Mohseni, M. Synthesis of photocatalytic nanosized TiO<sub>2</sub>-Ag particles with sol-gel method using reduction agent. *J. Mol. Catal. A: Chem.* **2005**, *242*, 135–140. [[CrossRef](#)]
59. Roy, P.; Ho, L.; Periasamy, A.P.; Lin, Y.; Huang, M.; Chang, H. Graphene-ZnO-Au nanocomposites based photocatalytic oxidation of benzoic acid. *ScienceJet* **2015**, *4*, 120.
60. Khedr, T.M.; El-Sheikh, S.M.; Hakki, A.; Ismail, A.A.; Badawy, W.A.; Bahnmann, D.W. Highly active non-metals doped mixed-phase TiO<sub>2</sub> for photocatalytic oxidation of ibuprofen under visible light. *J. Photochem. Photobiol. A Chem.* **2017**, *346*, 530–540. [[CrossRef](#)]
61. Yang, D.; Liu, H.; Zheng, Z.; Yuan, Y.; Zhao, J.C.; Waclawik, E.R.; Ke, X.; Zhu, H. An efficient photocatalyst structure: TiO<sub>2</sub> (B) nanofibers with a shell of anatase nanocrystals. *J. Am. Chem. Soc.* **2009**, *131*, 17885–17893. [[CrossRef](#)]
62. Kang, X.; Dong, G.; Dong, T. Oxygen Vacancy Defect Engineering of Heterophase Junction TiO<sub>2</sub>: Interfacial/Surface Oxygen Vacancies Coadjust the Photocatalytic ROS Production. *ACS Appl. Energy Mater.* **2022**, *6*, 1025–1036. [[CrossRef](#)]
63. Ding, L.; Yang, S.; Liang, Z.; Qian, X.; Chen, X.; Cui, H.; Tian, J. TiO<sub>2</sub> nanobelts with anatase/rutile heterophase junctions for highly efficient photocatalytic overall water splitting. *J. Colloid Interface Sci.* **2020**, *567*, 181–189. [[CrossRef](#)]
64. Berger, T.; Sterrer, M.; Diwald, O.; Knözinger, E.; Panayotov, D.; Thompson, T.L.; Yates, J.T. Light-induced charge separation in anatase TiO<sub>2</sub> particles. *J. Phys. Chem. B* **2005**, *109*, 6061–6068. [[CrossRef](#)]
65. Cao, F.; Xiong, J.; Wu, F.; Liu, Q.; Shi, Z.; Yu, Y.; Wang, X.; Li, L. Enhanced photoelectrochemical performance from rationally designed anatase/rutile TiO<sub>2</sub> heterostructures. *ACS Appl. Mater. Interfaces* **2016**, *8*, 12239–12245. [[CrossRef](#)]
66. Tian, G.; Fu, H.; Jing, L.; Xin, B.; Pan, K. Preparation and characterization of stable biphasic TiO<sub>2</sub> photocatalyst with high crystallinity, large surface area, and enhanced photoactivity. *J. Phys. Chem. C* **2008**, *112*, 3083–3089. [[CrossRef](#)]
67. Li, W.; Liu, C.; Zhou, Y.; Bai, Y.; Feng, X.; Yang, Z.; Lu, L.; Lu, X.; Chan, K.Y. Enhanced photocatalytic activity in anatase/TiO<sub>2</sub> (B) core-shell nanofiber. *J. Phys. Chem. C* **2008**, *112*, 20539–20545. [[CrossRef](#)]
68. Mu, R.; Ao, Y.; Wu, T.; Wang, C.; Wang, P. Synthesis of novel ternary heterogeneous anatase-TiO<sub>2</sub> (B) biphasic nanowires/Bi<sub>4</sub>O<sub>5</sub>I<sub>2</sub> composite photocatalysts for the highly efficient degradation of acetaminophen under visible light irradiation. *J. Hazard. Mater.* **2020**, *382*, 121083. [[CrossRef](#)]
69. Chen, J.; Guan, M.; Zhang, X.; Gong, X. Insights into a rutile/brookite homojunction of titanium dioxide: Separated reactive sites and boosted photocatalytic activity. *RSC Adv.* **2019**, *9*, 36615–36620. [[CrossRef](#)]
70. Fischer, K.; Gawel, A.; Rosen, D.; Krause, M.; Abdul Latif, A.; Griebel, J.; Prager, A.; Schulze, A. Low-temperature synthesis of anatase/rutile/brookite TiO<sub>2</sub> nanoparticles on a polymer membrane for photocatalysis. *Catalysts* **2017**, *7*, 209. [[CrossRef](#)]
71. An, X.; Hu, C.; Liu, H.; Qu, J. Hierarchical nanotubular anatase/rutile/TiO<sub>2</sub> (B) heterophase junction with oxygen vacancies for enhanced photocatalytic H<sub>2</sub> production. *Langmuir* **2018**, *34*, 1883–1889. [[CrossRef](#)]
72. Wang, C.; Zhang, X.; Liu, Y. Coexistence of an anatase/TiO<sub>2</sub> (B) heterojunction and an exposed (001) facet in TiO<sub>2</sub> nanoribbon photocatalysts synthesized via a fluorine-free route and topotactic transformation. *Nanoscale* **2014**, *6*, 5329–5337. [[CrossRef](#)] [[PubMed](#)]
73. Wang, Z.; Wang, Y.; Zhang, W.; Wang, Z.; Ma, Y.; Zhou, X. Fabrication of TiO<sub>2</sub> (B)/anatase heterophase junctions at high temperature via stabilizing the surface of TiO<sub>2</sub> (B) for enhanced photocatalytic activity. *J. Phys. Chem. C* **2019**, *123*, 1779–1789. [[CrossRef](#)]
74. Tanemura, S.; Miao, L.; Wunderlich, W.; Tanemura, M.; Mori, Y.; Toh, S.; Kaneko, K. Fabrication and characterization of anatase/rutile-TiO<sub>2</sub> thin films by magnetron sputtering: A review. *Sci. Technol. Adv. Mater.* **2005**, *6*, 11–17. [[CrossRef](#)]
75. Yamakata, A.; Vequizo, J.J.M. Curious behaviors of photogenerated electrons and holes at the defects on anatase, rutile, and brookite TiO<sub>2</sub> powders: A review. *J. Photochem. Photobiol. C Photochem. Rev.* **2019**, *40*, 234–243. [[CrossRef](#)]
76. Zhang, D.; Dong, S. Challenges in band alignment between semiconducting materials: A case of rutile and anatase TiO<sub>2</sub>. *Prog. Nat. Sci. Mater. Int.* **2019**, *29*, 277–284. [[CrossRef](#)]
77. Basavarajappa, P.S.; Patil, S.B.; Ganganagappa, N.; Reddy, K.R.; Raghu, A.V.; Reddy, C.V. Recent progress in metal-doped TiO<sub>2</sub>, non-metal doped/co-doped TiO<sub>2</sub> and TiO<sub>2</sub> nanostructured hybrids for enhanced photocatalysis. *Int. J. Hydrogen Energy* **2020**, *45*, 7764–7778. [[CrossRef](#)]
78. Connelly, K.; Wahab, A.K.; Idriss, H. Photoreaction of Au/TiO<sub>2</sub> for hydrogen production from renewables: A review on the synergistic effect between anatase and rutile phases of TiO<sub>2</sub>. *Mater. Renew. Sustain. Energy* **2012**, *1*, 1–12.
79. Mazierski, P.; Mikolajczyk, A.; Bajorowicz, B.; Malankowska, A.; Zaleska-Medynska, A.; Nadolna, J. The role of lanthanides in TiO<sub>2</sub>-based photocatalysis: A review. *Appl. Catal. B* **2018**, *233*, 301–317. [[CrossRef](#)]
80. Meng, A.; Zhang, L.; Cheng, B.; Yu, J. Dual cocatalysts in TiO<sub>2</sub> photocatalysis. *Adv. Mater.* **2019**, *31*, 1807660. [[CrossRef](#)]
81. Zaleska, A. Doped-TiO<sub>2</sub>: A review. *Recent Pat. Eng.* **2008**, *2*, 157–164. [[CrossRef](#)]
82. Adachi, S. *Physical Properties of III–V Semiconductor Compounds*; John Wiley & Sons: New York, NY, USA, 1992.
83. Ma, Y.; Wang, X.; Jia, Y.; Chen, X.; Han, H.; Li, C. Titanium dioxide-based nanomaterials for photocatalytic fuel generations. *Chem. Rev.* **2014**, *114*, 9987–10043. [[CrossRef](#)] [[PubMed](#)]
84. Smith, A.M.; Nie, S. Semiconductor nanocrystals: Structure, properties, and band gap engineering. *Acc. Chem. Res.* **2010**, *43*, 190–200. [[CrossRef](#)] [[PubMed](#)]

85. Sitt, A.; Hadar, I.; Banin, U. Band-gap engineering, optoelectronic properties and applications of colloidal heterostructured semiconductor nanorods. *Nano Today* **2013**, *8*, 494–513. [[CrossRef](#)]
86. Edgar, J.H. Prospects for device implementation of wide band gap semiconductors. *J. Mater. Res.* **1992**, *7*, 235–252. [[CrossRef](#)]
87. Ajmal, A.; Majeed, I.; Malik, R.N.; Idriss, H.; Nadeem, M.A. Principles and mechanisms of photocatalytic dye degradation on TiO<sub>2</sub> based photocatalysts: A comparative overview. *RSC Adv.* **2014**, *4*, 37003–37026. [[CrossRef](#)]
88. Guo, Q.; Zhou, C.; Ma, Z.; Yang, X. Fundamentals of TiO<sub>2</sub> photocatalysis: Concepts, mechanisms, and challenges. *Adv. Mater.* **2019**, *31*, 1901997. [[CrossRef](#)]
89. Linsebigler, A.L.; Lu, G.; Yates Jr, J.T. Photocatalysis on TiO<sub>2</sub> surfaces: Principles, mechanisms, and selected results. *Chem. Rev.* **1995**, *95*, 735–758. [[CrossRef](#)]
90. Kumar, A.; Khan, M.; He, J.; Lo, I.M. Recent developments and challenges in practical application of visible-light-driven TiO<sub>2</sub>-based heterojunctions for PPCP degradation: A critical review. *Water Res.* **2020**, *170*, 115356. [[CrossRef](#)]
91. Liu, L.; Li, Y. Understanding the reaction mechanism of photocatalytic reduction of CO<sub>2</sub> with H<sub>2</sub>O on TiO<sub>2</sub>-based photocatalysts: A review. *Aerosol Air Qual. Res.* **2014**, *14*, 453–469. [[CrossRef](#)]
92. Pawar, R.R.; Kim, M.; Kim, J.G.; Hong, S.M.; Sawant, S.Y.; Lee, S.M. Efficient removal of hazardous lead, cadmium, and arsenic from aqueous environment by iron oxide modified clay-activated carbon composite beads. *Appl. Clay Sci.* **2018**, *162*, 339–350. [[CrossRef](#)]
93. Zhang, J.; Tian, B.; Wang, L.; Xing, M.; Lei, J. Mechanism of photocatalysis. In *Photocatalysis: Fundamentals, Materials and Applications*; Zhang, J., Tian, B., Wang, L., Xing, M., Lei, J., Eds.; Springer: Singapore, 2018; pp. 1–15.
94. Regmi, C.; Joshi, B.; Ray, S.K.; Gyawali, G.; Pandey, R.P. Understanding mechanism of photocatalytic microbial decontamination of environmental wastewater. *Front. Chem.* **2018**, *6*, 33. [[CrossRef](#)] [[PubMed](#)]
95. Schneider, J.; Matsuoka, M.; Takeuchi, M.; Zhang, J.; Horiuchi, Y.; Anpo, M.; Bahnemann, D.W. Understanding TiO<sub>2</sub> photocatalysis: Mechanisms and materials. *Chem. Rev.* **2014**, *114*, 9919–9986. [[CrossRef](#)] [[PubMed](#)]
96. Wenderich, K.; Mul, G. Methods, mechanism, and applications of photodeposition in photocatalysis: A review. *Chem. Rev.* **2016**, *116*, 14587–14619. [[CrossRef](#)] [[PubMed](#)]
97. Zhu, T.; Ye, X.; Zhang, Q.; Hui, Z.; Wang, X.; Chen, S. Efficient utilization of photogenerated electrons and holes for photocatalytic redox reactions using visible light-driven Au/ZnIn<sub>2</sub>S<sub>4</sub> hybrid. *J. Hazard. Mater.* **2019**, *367*, 277–285. [[CrossRef](#)]
98. Gerischer, H. Electron-transfer kinetics of redox reactions at the semiconductor/electrolyte contact. A new approach. *J. Phys. Chem.* **1991**, *95*, 1356–1359. [[CrossRef](#)]
99. Hagfeldt, A.; Graetzel, M. Light-induced redox reactions in nanocrystalline systems. *Chem. Rev.* **1995**, *95*, 49–68. [[CrossRef](#)]
100. Ge, M.; Cao, C.; Huang, J.; Li, S.; Chen, Z.; Zhang, K.Q.; Al-Deyab, S.S.; Lai, Y. A review of one-dimensional TiO<sub>2</sub> nanostructured materials for environmental and energy applications. *J. Mater. Chem. A* **2016**, *4*, 6772–6801. [[CrossRef](#)]
101. Ahmed, S.; Rasul, M.G.; Martens, W.N.; Brown, R.; Hashib, M.A. Heterogeneous photocatalytic degradation of phenols in wastewater: A review on current status and developments. *Desalination* **2010**, *261*, 3–18. [[CrossRef](#)]
102. Nosaka, Y.; Nosaka, A.Y. Generation and Detection of Reactive Oxygen Species in Photocatalysis. *Chem. Rev.* **2017**, *117*, 11302–11336. [[CrossRef](#)]
103. Feng, X.; Guo, H.; Patel, K.; Zhou, H.; Lou, X. High performance, recoverable Fe<sub>3</sub>O<sub>4</sub>ZnO nanoparticles for enhanced photocatalytic degradation of phenol. *Chem. Eng. J.* **2014**, *244*, 327–334. [[CrossRef](#)]
104. Zhang, J.; Nosaka, Y. Mechanism of the OH radical generation in photocatalysis with TiO<sub>2</sub> of different crystalline types. *J. Phys. Chem. C* **2014**, *118*, 10824–10832. [[CrossRef](#)]
105. Sobczyński, A.; Duczmal, Ł.; Zmudziński, W. Phenol destruction by photocatalysis on TiO<sub>2</sub>: An attempt to solve the reaction mechanism. *J. Mol. Catal. A Chem.* **2004**, *213*, 225–230. [[CrossRef](#)]
106. Gong, M.; Xiao, S.; Yu, X.; Dong, C.; Ji, J.; Zhang, D.; Xing, M. Research progress of photocatalytic sterilization over semiconductors. *RSC Adv.* **2019**, *9*, 19278–19284. [[CrossRef](#)] [[PubMed](#)]
107. Dambournet, D.; Belharouak, I.; Amine, K. Tailored preparation methods of TiO<sub>2</sub> anatase, rutile, brookite: Mechanism of formation and electrochemical properties. *Chem. Mater.* **2010**, *22*, 1173–1179. [[CrossRef](#)]
108. Reyes-Coronado, D.; Rodríguez-Gattorno, G.; Espinosa-Pesqueira, M.E.; Cab, C.; De Coss, R.D.; Oskam, G. Phase-pure TiO<sub>2</sub> nanoparticles: Anatase, brookite and rutile. *Nanotechnology* **2008**, *19*, 145605. [[CrossRef](#)]
109. Tompsett, G.A.; Bowmaker, G.A.; Cooney, R.P.; Metson, J.B.; Rodgers, K.A.; Seakins, J.M. The Raman spectrum of brookite, TiO<sub>2</sub> (PBCA, Z = 8). *J. Raman Spectrosc.* **1995**, *26*, 57–62. [[CrossRef](#)]
110. Beltran, A.; Gracia, L.; Andres, J. Density functional theory study of the brookite surfaces and phase transitions between natural titania polymorphs. *J. Phys. Chem. B* **2006**, *110*, 23417–23423. [[CrossRef](#)]
111. Monai, M.; Montini, T.; Fornasiero, P. Brookite: Nothing new under the sun? *Catalysts* **2017**, *7*, 304. [[CrossRef](#)]
112. Li, Z.; Cong, S.; Xu, Y. Brookite vs anatase TiO<sub>2</sub> in the photocatalytic activity for organic degradation in water. *ACS Catal.* **2014**, *4*, 3273–3280. [[CrossRef](#)]
113. Banfield, J.F.; Veblen, D.R.; Smith, D.J. The identification of naturally occurring TiO<sub>2</sub> (B) by structure determination using high-resolution electron microscopy, image simulation, and distance-least-squares refinement. *Am. Mineral.* **1991**, *76*, 343–353.
114. Xiang, G.; Wang, Y.G.; Li, J.; Zhuang, J.; Wang, X. Surface-specific interaction by structure-match confined pure high-energy facet of unstable TiO<sub>2</sub> (B) polymorph. *Sci. Rep.* **2013**, *3*, 1411. [[CrossRef](#)] [[PubMed](#)]

115. Armstrong, A.R.; Armstrong, G.; Canales, J.; Bruce, P.G. TiO<sub>2</sub>-B nanowires. *Angew. Chem. Int. Ed.* **2004**, *43*, 2286–2288. [[CrossRef](#)] [[PubMed](#)]
116. Nosheen, S.; Galasso, F.S.; Suib, S.L. Role of Ti-O bonds in phase transitions of TiO<sub>2</sub>. *Langmuir* **2009**, *25*, 7623–7630. [[CrossRef](#)] [[PubMed](#)]
117. Opra, D.P.; Gnedenkov, S.V.; Sinebryukhov, S.L. Recent efforts in design of TiO<sub>2</sub> (B) anodes for high-rate lithium-ion batteries: A review. *J. Power Sources* **2019**, *442*, 227225. [[CrossRef](#)]
118. Kim, W.; Tachikawa, T.; Moon, G.H.; Majima, T.; Choi, W. Molecular-level understanding of the photocatalytic activity difference between anatase and rutile Nanoparticles. *Angew. Chem.* **2014**, *126*, 14260–14265. [[CrossRef](#)]
119. Sclafani, A.; Herrmann, J.M. Comparison of the photoelectronic and photocatalytic activities of various anatase and rutile forms of titania in pure liquid organic phases and in aqueous solutions. *J. Phys. Chem.* **1996**, *100*, 13655–13661. [[CrossRef](#)]
120. Zhang, J.; Zhou, P.; Liu, J.; Yu, J. New understanding of the difference of photocatalytic activity among anatase, rutile and brookite TiO<sub>2</sub>. *Phys. Chem. Chem. Phys.* **2014**, *16*, 20382–20386. [[CrossRef](#)]
121. Wu, X.; Ng, Y.H.; Wang, L.; Du, Y.; Dou, S.X.; Amal, R.; Scott, J. Improving the photo-oxidative capability of BiOBr via crystal facet engineering. *J. Mater. Chem. A* **2017**, *5*, 8117–8124. [[CrossRef](#)]
122. Zhang, L.; Ran, J.; Qiao, S.Z.; Jaroniec, M. Characterization of semiconductor photocatalysts. *Chem. Soc. Rev.* **2019**, *48*, 5184–5206. [[CrossRef](#)]
123. Wang, L.; Zhao, J.; Liu, H.; Huang, J. Design, modification and application of semiconductor photocatalysts. *J. Taiwan Inst. Chem. Eng.* **2018**, *93*, 590–602. [[CrossRef](#)]
124. Comparelli, R.; Fanizza, E.; Curri, M.L.; Cozzoli, P.D.; Mascolo, G.; Passino, R.; Agostiano, A. Photocatalytic degradation of azo dyes by organic-capped anatase TiO<sub>2</sub> nanocrystals immobilized onto substrates. *Appl. Catal. B* **2005**, *55*, 81–91. [[CrossRef](#)]
125. Katal, R.; Masudy-Panah, S.; Tanhaei, M.; Farahani, M.H.D.A.; Jiangyong, H. A review on the synthesis of the various types of anatase TiO<sub>2</sub> facets and their applications for photocatalysis. *Chem. Eng. J.* **2020**, *384*, 123384. [[CrossRef](#)]
126. Porkodi, K.; Arokiamary, S.D. Synthesis and spectroscopic characterization of nanostructured anatase titania: A photocatalyst. *Mater. Charact.* **2007**, *58*, 495–503. [[CrossRef](#)]
127. Sivalingam, G.; Nagaveni, K.; Hegde, M.S.; Madras, G. Photocatalytic degradation of various dyes by combustion synthesized nano anatase TiO<sub>2</sub>. *Appl. Catal. B* **2003**, *45*, 23–38. [[CrossRef](#)]
128. Periyat, P.; Naufal, B.; Ullattil, S.G. A review on high temperature stable anatase TiO<sub>2</sub> photocatalysts. *Mater. Sci. Forum* **2016**, *855*, 78–93. [[CrossRef](#)]
129. Nosaka, Y.; Nosaka, A.Y. Reconsideration of intrinsic band alignments within anatase and rutile TiO<sub>2</sub>. *J. Phys. Chem. Lett.* **2016**, *7*, 431–434. [[CrossRef](#)]
130. Yuan, L.D.; Deng, H.X.; Li, S.S.; Wei, S.H.; Luo, J.W. Unified theory of direct or indirect band-gap nature of conventional semiconductors. *Phys. Rev. B* **2018**, *98*, 245203. [[CrossRef](#)]
131. Gu, L.; Srot, V.; Sigle, W.; Koch, C.; van Aken, P.; Scholz, F.; Thapa, S.B.; Kirchner, C.; Jetter, M.; Rühle, M. Band-gap measurements of direct and indirect semiconductors using monochromated electrons. *Phys. Rev. B* **2007**, *75*, 195214. [[CrossRef](#)]
132. López, R.; Gómez, R. Band-gap energy estimation from diffuse reflectance measurements on sol-gel and commercial TiO<sub>2</sub>: A comparative study. *J. Sol-Gel Sci. Technol.* **2012**, *61*, 1–7. [[CrossRef](#)]
133. Zhou, W.; Umezawa, N.; Ma, R.; Sakai, N.; Ebina, Y.; Sano, K.; Liu, M.; Ishida, Y.; Aida, T.; Sasaki, T. Spontaneous direct band gap, high hole mobility, and huge exciton energy in atomic-thin TiO<sub>2</sub> nanosheet. *Chem. Mater.* **2018**, *30*, 6449–6457. [[CrossRef](#)]
134. Wetchakun, N.; Incessungvorn, B.; Wetchakun, K.; Phanichphant, S. Influence of calcination temperature on anatase to rutile phase transformation in TiO<sub>2</sub> nanoparticles synthesized by the modified sol-gel method. *Mater. Lett.* **2012**, *82*, 195–198. [[CrossRef](#)]
135. Bagheri, S.; Julkapli, N.M. Mixed-phase TiO<sub>2</sub> photocatalysis: Correlation between phase composition and photodecomposition of water pollutants. *Rev. Inorg. Chem.* **2017**, *37*, 11–28. [[CrossRef](#)]
136. Ou, X.; Liu, X.; Liu, W.; Rong, W.; Li, J.; Lin, Z. Surface defects enhance the adsorption affinity and selectivity of Mg(OH)<sub>2</sub> towards As (V) and Cr (VI) oxyanions: A combined theoretical and experimental study. *Environ. Sci. Nano* **2018**, *5*, 2570–2578. [[CrossRef](#)]
137. Yang, H.G.; Sun, C.H.; Qiao, S.Z.; Zou, J.; Liu, G.; Smith, S.C.; Cheng, H.M.; Lu, G.Q. Anatase TiO<sub>2</sub> single crystals with a large percentage of reactive facets. *Nature* **2008**, *453*, 638–641. [[CrossRef](#)] [[PubMed](#)]
138. Fagan, R.; Synnott, D.W.; McCormack, D.E.; Pillai, S.C. An effective method for the preparation of high temperature stable anatase TiO<sub>2</sub> photocatalysts. *Appl. Surf. Sci.* **2016**, *371*, 447–452. [[CrossRef](#)]
139. Bubacz, K.; Choina, J.; Dolat, D.; Morawski, A.W. Methylene Blue and Phenol Photocatalytic Degradation on Nanoparticles of Anatase TiO<sub>2</sub>. *Pol. J. Environ. Stud.* **2010**, *19*, 685–691.
140. Etacheri, V.; Seery, M.K.; Hinder, S.J.; Pillai, S.C. Oxygen rich titania: A dopant free, high temperature stable, and visible-light active anatase photocatalyst. *Adv. Funct. Mater.* **2011**, *21*, 3744–3752. [[CrossRef](#)]
141. Lv, K.; Cheng, B.; Yu, J.; Liu, G. Fluorine ions-mediated morphology control of anatase TiO<sub>2</sub> with enhanced photocatalytic activity. *Phys. Chem. Chem. Phys.* **2012**, *14*, 5349–5362. [[CrossRef](#)]
142. Wang, X.; Kafizas, A.; Li, X.; Moniz, S.J.; Reardon, P.J.; Tang, J.; Parkin, I.P.; Durrant, J.R. Transient absorption spectroscopy of anatase and rutile: The impact of morphology and phase on photocatalytic activity. *J. Phys. Chem. C* **2015**, *119*, 10439–10447. [[CrossRef](#)]
143. Bickley, R.I.; Stone, F.S. Photoadsorption and photocatalysis at rutile surfaces: I. Photoadsorption of oxygen. *J. Catal.* **1973**, *31*, 389–397. [[CrossRef](#)]

144. Bickley, R.I.; Munuera, G.; Stone, F.S. Photoadsorption and photocatalysis at rutile surfaces: II. Photocatalytic oxidation of isopropanol. *J. Catal.* **1973**, *31*, 398–407. [[CrossRef](#)]
145. Amano, F.; Nakata, M.; Yamamoto, A.; Tanaka, T. Rutile titanium dioxide prepared by hydrogen reduction of Degussa P25 for highly efficient photocatalytic hydrogen evolution. *Catal. Sci. Technol.* **2016**, *6*, 5693–5699. [[CrossRef](#)]
146. Shi, J.; Chen, J.; Feng, Z.; Chen, T.; Lian, Y.; Wang, X.; Li, C. Photoluminescence characteristics of TiO<sub>2</sub> and their relationship to the photoassisted reaction of water/methanol mixture. *J. Phys. Chem. C* **2007**, *111*, 693–699. [[CrossRef](#)]
147. Park, N.G.; Van de Lagemaat, J.; Frank, A.A. Comparison of dye-sensitized rutile-and anatase-based TiO<sub>2</sub> solar cells. *J. Phys. Chem. B* **2000**, *104*, 8989–8994. [[CrossRef](#)]
148. Zhao, J.; Liu, S.; Zhang, X.; Xu, Y. Different effects of fluoride and phosphate anions on TiO<sub>2</sub> photocatalysis (rutile). *Catal. Sci. Technol.* **2020**, *10*, 6552–6561. [[CrossRef](#)]
149. Wang, Y.; Zhang, L.; Deng, K.; Chen, X.; Zou, Z. Low temperature synthesis and photocatalytic activity of rutile TiO<sub>2</sub> nanorod superstructures. *J. Phys. Chem. C* **2007**, *111*, 2709–2714. [[CrossRef](#)]
150. Miyoshi, A.; Nishioka, S.; Maeda, K. Water splitting on rutile TiO<sub>2</sub>-based photocatalysts. *Chem. Eur. J.* **2018**, *24*, 18204–18219. [[CrossRef](#)]
151. Liu, Q.Y.; Wang, H.D.; Tang, R.; Cheng, Q.; Yuan, Y.J. Rutile TiO<sub>2</sub> nanoparticles with oxygen vacancy for photocatalytic nitrogen fixation. *ACS Appl. Nano Mater.* **2021**, *4*, 8674–8679. [[CrossRef](#)]
152. Yurdakal, S.; Palmisano, G.; Loddo, V.; Augugliaro, V.; Palmisano, L. Nanostructured rutile TiO<sub>2</sub> for selective photocatalytic oxidation of aromatic alcohols to aldehydes in water. *J. Am. Chem. Soc.* **2008**, *130*, 1568–1569. [[CrossRef](#)]
153. Jung, H.S.; Kim, H. Origin of low photocatalytic activity of rutile TiO<sub>2</sub>. *Electron. Mater. Lett.* **2009**, *5*, 73–76. [[CrossRef](#)]
154. Zhao, Z.; Zhang, X.; Zhang, G.; Liu, Z.; Qu, D.; Miao, X.; Feng, P.; Sun, Z. Effect of defects on photocatalytic activity of rutile TiO<sub>2</sub> nanorods. *Nano Res.* **2015**, *8*, 4061–4071. [[CrossRef](#)]
155. Djokić, V.R.; Marinković, A.D.; Petrović, R.D.; Ersen, O.; Zafeiratos, S.; Mitrić, M.; Ophus, C.; Radmilović, V.R.; Janačković, D.T. Highly active rutile TiO<sub>2</sub> nanocrystalline photocatalysts. *ACS Appl. Mater. Interfaces* **2020**, *12*, 33058–33068. [[CrossRef](#)] [[PubMed](#)]
156. Zhang, J.; Song, Y.; Lu, F.; Fei, W.; Mengqiong, Y.; Genxiang, L.; Qian, X.; Xiang, W.; Can, L. Photocatalytic degradation of rhodamine B on anatase, rutile, and brookite TiO<sub>2</sub>. *Chinese J. Catal.* **2011**, *32*, 983–991. [[CrossRef](#)]
157. Pauling, L.; Sturdivant, J.H., XV. The crystal structure of brookite. *Z. Kristallogr. Cryst. Mater.* **1928**, *68*, 239–256. [[CrossRef](#)]
158. Di Paola, A.; Bellardita, M.; Palmisano, L. Brookite, the least known TiO<sub>2</sub> photocatalyst. *Catalysts* **2013**, *3*, 36–73. [[CrossRef](#)]
159. Zhang, H.; Banfield, J.F. Understanding polymorphic phase transformation behavior during growth of nanocrystalline aggregates: Insights from TiO<sub>2</sub>. *J. Phys. Chem. B* **2000**, *104*, 3481–3487. [[CrossRef](#)]
160. Xie, J.; Lü, X.; Liu, J.; Shu, H. Brookite titania photocatalytic nanomaterials: Synthesis, properties, and applications. *Pure Appl. Chem.* **2009**, *81*, 2407–2415. [[CrossRef](#)]
161. Thuong, H.T.T.; Kim, C.T.T.; Quang, L.N.; Kosslick, H. Highly active brookite TiO<sub>2</sub>-assisted photocatalytic degradation of dyes under the simulated solar–UVA radiation. *Prog. Nat. Sci. Mater. Int.* **2019**, *29*, 641–647. [[CrossRef](#)]
162. Kandiell, T.A.; Robben, L.; Alkaima, A.; Bahnemann, D. Brookite versus anatase TiO<sub>2</sub> photocatalysts: Phase transformations and photocatalytic activities. *Photochem. Photobiol. Sci.* **2013**, *12*, 602–609. [[CrossRef](#)]
163. Khan, S.; Je, M.; Kim, D.; Lee, S.; Cho, S.H.; Song, T.; Choi, H. Mapping point defects of brookite TiO<sub>2</sub> for photocatalytic activity beyond anatase and P25. *J. Phys. Chem. C* **2020**, *124*, 10376–10384. [[CrossRef](#)]
164. Zhuang, B.; Shi, H.; Zhang, H.; Zhang, Z. Sodium doping in brookite TiO<sub>2</sub> enhances its photocatalytic activity. *Beilstein J. Nanotechnol.* **2022**, *13*, 599–609. [[CrossRef](#)] [[PubMed](#)]
165. Žerjav, G.; Žižek, K.; Zavašnik, J.; Pintar, A. Brookite vs. rutile vs. anatase: Whats behind their various photocatalytic activities? *J. Environ. Chem. Eng.* **2022**, *10*, 107722. [[CrossRef](#)]
166. Bellardita, M.; Di Paola, A.; Megna, B.; Palmisano, L. Absolute crystallinity and photocatalytic activity of brookite TiO<sub>2</sub> samples. *Appl. Catal. B* **2017**, *201*, 150–158. [[CrossRef](#)]
167. Choi, M.; Lim, J.; Baek, M.; Choi, W.; Kim, W.; Yong, K. Investigating the unrevealed photocatalytic activity and stability of nanostructured brookite TiO<sub>2</sub> film as an environmental photocatalyst. *ACS Appl. Mater. Interfaces* **2017**, *9*, 16252–16260. [[CrossRef](#)]
168. Do, H.H.; Tran, T.K.C.; Ung, T.D.T.; Dao, N.T.; Nguyen, D.D.; Trinh, T.H.; Hoang, T.D.; Le, T.L.; Tran, T.T.H. Controllable fabrication of photocatalytic TiO<sub>2</sub> brookite thin film by 3D-printing approach for dyes decomposition. *J. Water Process. Eng.* **2021**, *43*, 102319. [[CrossRef](#)]
169. Marchand, R.; Brohan, L.; Tournoux, M. TiO<sub>2</sub> (B) a new form of titanium dioxide and the potassium octatitanate K<sub>2</sub>Ti<sub>8</sub>O<sub>17</sub>. *Mater. Res. Bull.* **1980**, *15*, 1129–1133. [[CrossRef](#)]
170. Dylla, A.G.; Henkelman, G.; Stevenson, K.J. Lithium insertion in nanostructured TiO<sub>2</sub> (B) architectures. *Acc. Chem. Res.* **2013**, *46*, 1104–1112. [[CrossRef](#)]
171. Fehse, M.; Ventosa, E. Is TiO<sub>2</sub> (B) the future of titanium-based battery materials? *ChemPlusChem* **2015**, *80*, 785–795. [[CrossRef](#)] [[PubMed](#)]
172. Hua, X.; Liu, Z.; Bruce, P.G.; Grey, C.P. The morphology of TiO<sub>2</sub> (B) nanoparticles. *J. Am. Chem. Soc.* **2015**, *137*, 13612–13623. [[CrossRef](#)] [[PubMed](#)]
173. Liu, S.; Jia, H.; Han, L.; Wang, J.; Gao, P.; Xu, D.; Yang, J.; Che, S. Nanosheet-constructed porous TiO<sub>2</sub>-B for advanced lithium-ion batteries. *Adv. Mater.* **2012**, *24*, 3201–3204. [[CrossRef](#)] [[PubMed](#)]

174. Ren, Y.; Liu, Z.; Pourpoint, F.; Armstrong, A.R.; Grey, C.P.; Bruce, P.G. Nanoparticulate TiO<sub>2</sub> (B): An anode for lithium-ion batteries. *Angew. Chem.* **2012**, *124*, 2206–2209. [[CrossRef](#)]
175. Chakraborty, A.K.; Qi, Z.; Chai, S.Y.; Lee, C.; Park, S.Y.; Jang, D.J.; Lee, W.I. Formation of highly crystallized TiO<sub>2</sub> (B) and its photocatalytic behavior. *Appl. Catal. B* **2010**, *93*, 368–375. [[CrossRef](#)]
176. Zhang, Y.; Xing, Z.; Liu, X.; Li, Z.; Wu, X.; Jiang, J.; Li, M.; Zhu, Q.; Zhou, W. Ti<sup>3+</sup> self-doped blue TiO<sub>2</sub> (B) single-crystalline nanorods for efficient solar-driven photocatalytic performance. *ACS Appl. Mater. Interfaces* **2016**, *8*, 26851–26859. [[CrossRef](#)] [[PubMed](#)]
177. Lee, J.S.; You, K.H.; Park, C.B. Highly photoactive, low bandgap TiO<sub>2</sub> nanoparticles wrapped by graphene. *Adv. Mater.* **2012**, *24*, 1084–1088. [[CrossRef](#)] [[PubMed](#)]
178. Peighambaroust, N.S.; Khameneh Asl, S.; Mohammadpour, R.; Asl, S.K. Band-gap narrowing and electrochemical properties in N-doped and reduced anodic TiO<sub>2</sub> nanotube arrays. *Electrochim. Acta* **2018**, *270*, 245–255. [[CrossRef](#)]
179. Sharma, P.K.; Cortes, M.A.L.R.M.; Hamilton, J.W.J.; Han, Y.; Byrne, J.A.; Nolan, M. Surface modification of TiO<sub>2</sub> with copper clusters for band gap narrowing. *Catal. Today* **2017**, *321–322*, 9–17. [[CrossRef](#)]
180. Vargas Hernández, J.; Coste, S.; García Murillo, A.; Carrillo Romo, F.; Kassiba, A. Effects of metal doping (Cu, Ag, Eu) on the electronic and optical behavior of nanostructured TiO<sub>2</sub>. *J. Alloys Compd.* **2017**, *710*, 355–363. [[CrossRef](#)]
181. Zhang, J.; Tian, B.; Wang, L.; Xing, M. *Photocatalysis*; Springer: Singapore, 2018.
182. Huang, Y.; Cao, J.J.; Kang, F.; You, S.J.; Chang, C.W.; Wang, Y.F. High selectivity of visible-light-driven La-doped TiO<sub>2</sub> photocatalysts for NO removal. *Aerosol Air Qual. Res.* **2017**, *17*, 2555–2565. [[CrossRef](#)]
183. Marques, J.; Gomes, T.D.; Forte, M.A.; Silva, R.F.; Tavares, C.J. A new route for the synthesis of highly-active N-doped TiO<sub>2</sub> nanoparticles for visible light photocatalysis using urea as nitrogen precursor. *Catal. Today* **2019**, *326*, 36–45. [[CrossRef](#)]
184. Liu, D.; Tian, R.; Wang, J.; Nie, E.; Piao, X.; Li, X.; Sun, Z. Photoelectrocatalytic degradation of methylene blue using F doped TiO<sub>2</sub> photoelectrode under visible light irradiation. *Chemosphere* **2017**, *185*, 574–581. [[CrossRef](#)]
185. Boningari, T.; Inturi, S.N.R.; Suidan, M.; Smirniotis, P.G. Novel one-step synthesis of sulfur doped-TiO<sub>2</sub> by flame spray pyrolysis for visible light photocatalytic degradation of acetaldehyde. *Chem. Eng. J.* **2018**, *339*, 249–258. [[CrossRef](#)]
186. Payormhorm, J.; Idem, R. Synthesis of C-doped TiO<sub>2</sub> by sol-microwave method for photocatalytic conversion of glycerol to value-added chemicals under visible light. *Appl. Catal. A-Gen.* **2020**, *590*, 117362. [[CrossRef](#)]
187. Nagaraj, G.; Raj, A.D.; Irudayaraj, A.A.; Josephine, R.L. Tuning the optical band Gap of pure TiO<sub>2</sub> via photon induced method. *Optik* **2018**, *179*, 889–894.
188. Hu, J.; Zhang, S.; Cao, Y.; Wang, H.; Yu, H.; Peng, F. Novel highly active anatase/rutile TiO<sub>2</sub> photocatalyst with hydrogenated heterophase interface structures for photoelectrochemical water splitting into hydrogen. *ACS Sustain. Chem. Eng.* **2018**, *6*, 10823–10832. [[CrossRef](#)]
189. Lu, S.; Yang, S.; Hu, X.; Liang, Z.; Guo, Y.; Xue, Y.; Cui, H.; Tian, J. Fabrication of TiO<sub>2</sub> nanoflowers with bronze (TiO<sub>2</sub> (B))/anatase heterophase junctions for efficient photocatalytic hydrogen production. *Int. J. Hydrogen Energy* **2019**, *44*, 24398–24406. [[CrossRef](#)]
190. Jimenez-Relinque, E.; Castellote, M. Hydroxyl radical and free and shallowly trapped electron generation and electron/hole recombination rates in TiO<sub>2</sub> photocatalysis using different combinations of anatase and rutile. *Appl. Catal. A-Gen.* **2018**, *565*, 20–25. [[CrossRef](#)]
191. Xu, X.; Guo, Y.; Liang, Z.; Cui, H.; Tian, J. Remarkable charge separation and photocatalytic efficiency enhancement through TiO<sub>2</sub> (B)/anatase heterophase junctions of TiO<sub>2</sub> nanobelts. *Int. J. Hydrogen Energy* **2019**, *44*, 27311–27318. [[CrossRef](#)]
192. Ruan, X.; Cui, X.; Cui, Y.; Fan, X.; Li, Z.; Xie, T.; Ba, K.; Jia, G.; Zhang, H.; Zhang, L.; et al. Favorable energy band alignment of TiO<sub>2</sub> anatase/rutile heterophase homojunctions yields photocatalytic hydrogen evolution with quantum efficiency exceeding 45.6%. *Adv. Energy Mater.* **2022**, *12*, 2200298. [[CrossRef](#)]
193. Foster, H.A.; Ditta, I.B.; Varghese, S.; Steele, A. Photocatalytic disinfection using titanium dioxide: Spectrum and mechanism of antimicrobial activity. *Appl. Microbiol. Biotechnol.* **2011**, *90*, 1847–1868. [[CrossRef](#)]
194. Zhang, C.; Li, Y.; Shuai, D.; Shen, Y.; Wang, D. Progress and challenges in photocatalytic disinfection of waterborne Viruses: A review to fill current knowledge gaps. *Chem. Eng. J.* **2019**, *355*, 399–415. [[CrossRef](#)]
195. Luo, Z.; Poyraz, A.S.; Kuo, C.H.; Miao, R.; Meng, Y.; Chen, S.Y.; Jiang, T.; Wenos, C.; Suib, S.L. Crystalline mixed phase (anatase/rutile) mesoporous titanium dioxides for visible light photocatalytic activity. *Chem. Mater.* **2015**, *27*, 6–17. [[CrossRef](#)]
196. Franciosi, A.; Van de Walle, C.G. Heterojunction band offset engineering. *Surf. Sci. Rep.* **1996**, *25*, 1–140. [[CrossRef](#)]
197. Tung, R.T.; Kronik, L. Charge density and band offsets at heterovalent semiconductor interfaces. *Adv. Theory Simul.* **2018**, *1*, 1700001. [[CrossRef](#)]
198. Scanlon, D.O.; Dunnill, C.W.; Buckeridge, J.; Shevlin, S.A.; Logsdail, A.J.; Woodley, S.M.; Catlow, C.R.A.; Powell, M.; Palgrave, R.G.; Parkin, I.P.; et al. Band alignment of rutile and anatase TiO<sub>2</sub>. *Nat. Mater.* **2013**, *12*, 798–801. [[CrossRef](#)] [[PubMed](#)]
199. Singh, M.K.; Mehata, M.S. Phase-dependent optical and photocatalytic performance of synthesized titanium dioxide (TiO<sub>2</sub>) nanoparticles. *Optik* **2019**, *193*, 163011. [[CrossRef](#)]
200. Sato, T.; Taya, M. Enhancement of phage inactivation using photocatalytic titanium dioxide particles with different crystalline structures. *Biochem. Eng. J.* **2006**, *28*, 303–308. [[CrossRef](#)]
201. Zhu, W.; Kong, L.; Long, W.; Shi, X.; Zhou, D.; Sun, L.; Zhou, L.; Yang, G.; Liu, X.; Liu, H.; et al. Band Structure Engineering of Black Phosphorus/Graphene/MoS<sub>2</sub> van der Waals Heterojunctions for Photovoltaic and Op-toelectronic Device Application. *J. Phys. Conf. Ser.* **2021**, *1865*, 022021. [[CrossRef](#)]

202. Sun, X.; Chang, Y.; Cheng, Y.; Feng, Y.; Zhang, H. Band alignment-driven oxidative injury to the skin by anatase/rutile mixed-phase titanium dioxide nanoparticles under sunlight exposure. *Toxicol. Sci.* **2018**, *164*, 300–312. [[CrossRef](#)]
203. Zhang, Z.; Yates, J.T., Jr. Band bending in semiconductors: Chemical and physical consequences at surfaces and interfaces. *Chem. Rev.* **2012**, *112*, 5520–5551. [[CrossRef](#)]
204. Vittadini, A.; Casarin, M.; Selloni, A. Chemistry of and on TiO<sub>2</sub>-anatase surfaces by DFT calculations: A partial review. *Theor. Chem. Acc.* **2007**, *117*, 663–671. [[CrossRef](#)]
205. Ju, M.G.; Sun, G.; Wang, J.; Meng, Q.; Liang, W. Origin of high photocatalytic properties in the mixed-phase TiO<sub>2</sub>: A first-principles theoretical study. *ACS Appl. Mater. Interfaces* **2014**, *6*, 12885–12892. [[CrossRef](#)] [[PubMed](#)]
206. Deskins, N.A.; Kerisit, S.; Rosso, K.M.; Dupuis, M. Molecular dynamics characterization of rutile-anatase interfaces. *J. Phys. Chem. C* **2007**, *111*, 9290–9298. [[CrossRef](#)]
207. Davlatshoevich, N.D.; Ashur, K.M.; Saidali, B.A.; Kholmirtzotagoykulovich, K.; Lyubchyk, A.; Ibrahim, M. Investigation of structural and optoelectronic properties of N-doped hexagonal phases of TiO<sub>2</sub> (TiO<sub>2-x</sub>N<sub>x</sub>) nanoparticles with DFT realization: Optimization of the band gap and optical properties for visible-light absorption and photovoltaic applications. *Biointerface Res. Appl. Chem.* **2022**, *12*, 3836–3848.
208. Liang, B.; Mianxin, S.; Tianliang, Z.; Xiaoyong, Z.; Qingqing, D. Band gap calculation and photo catalytic activity of rare earths doped rutile TiO<sub>2</sub>. *J. Rare Earths* **2009**, *27*, 461–468.
209. Quesada-Cabrera, R.; Sotelo-Vazquez, C.; Bear, J.C.; Darr, J.A.; Parkin, I.P. Photocatalytic Evidence of the Rutile-to-Anatase Electron Transfer in Titania. *Adv. Mater. Interfaces* **2014**, *1*, 1400069. [[CrossRef](#)]
210. Ullattil, S.G.; Periyat, P. Sol-gel synthesis of titanium dioxide. In *Sol-Gel Materials for Energy, Environment and Electronic Applications*; Pillai, S.C., Hehir, S., Eds.; Springer Cham: New York, NY, USA, 2017; pp. 271–283.
211. Wang, C.C.; Ying, J.Y. Sol-gel synthesis and hydrothermal processing of anatase and rutile titania nanocrystals. *Chem. Mater.* **1999**, *11*, 3113–3120. [[CrossRef](#)]
212. Permana, M.D.; Noviyanti, A.R.; Lestari, P.R.; Kumada, N.; Eddy, D.R.; Rahayu, I. Enhancing the photocatalytic activity of TiO<sub>2</sub>/Na<sub>2</sub>Ti<sub>6</sub>O<sub>13</sub> composites by gold for the photodegradation of phenol. *ChemEngineering* **2022**, *6*, 69. [[CrossRef](#)]
213. Arnal, P.; Corriu, R.J.; Leclercq, D.; Mutin, P.H.; Vioux, A. Preparation of anatase, brookite and rutile at low temperature by non-hydrolytic sol-gel methods. *J. Mater. Chem.* **1996**, *6*, 1925–1932. [[CrossRef](#)]
214. Castrejón-Sánchez, V.H.; López, R.; Ramón-González, M.; Enríquez-Pérez, Á.; Camacho-López, M.; Villa-Sánchez, G. Annealing control on the anatase/rutile ratio of nanostructured titanium dioxide obtained by sol-gel. *Crystals* **2018**, *9*, 22. [[CrossRef](#)]
215. Noviyanti, A.R.; Asyiah, E.N.; Permana, M.D.; Dwiyantri, D.; Eddy, D.R. Preparation of Hydroxyapatite-Titanium Dioxide Composite from Eggshell by Hydrothermal Method: Characterization and Antibacterial Activity. *Crystals* **2022**, *12*, 1599. [[CrossRef](#)]
216. Aruna, S.T.; Tirosh, S.; Zaban, A. Nanosize rutile titania particle synthesis via hydrothermal method without mineralizers. *J. Mater. Chem.* **2000**, *10*, 2388–2391. [[CrossRef](#)]
217. Li, G.; Ciston, S.; Saponjic, Z.V.; Chen, L.; Dimitrijevic, N.M.; Rajh, T.; Gray, K.A. Synthesizing mixed-phase TiO<sub>2</sub> nanocomposites using a hydrothermal method for photo-oxidation and photoreduction applications. *J. Catal.* **2008**, *253*, 105–110. [[CrossRef](#)]
218. Sun, C.; Wang, N.; Zhou, S.; Hu, X.; Zhou, S.; Chen, P. Preparation of self-supporting hierarchical nanostructured anatase/rutile composite TiO<sub>2</sub> film. *Chem. Comm.* **2008**, *28*, 3293–3295. [[CrossRef](#)] [[PubMed](#)]
219. Bao, Y.; Wei, P.; Xia, X.; Huang, Z.; Homewood, K.; Gao, Y. Remarkably enhanced H<sub>2</sub> response and detection range in Nb doped rutile/anatase heterophase junction TiO<sub>2</sub> thin film hydrogen sensors. *Sens. Actuators B Chem.* **2019**, *301*, 127143. [[CrossRef](#)]
220. He, J.; Du, Y.; Bai, Y.; An, J.; Cai, X.; Chen, Y.; Wang, P.; Yang, X.; Feng, Q. Facile formation of anatase/rutile TiO<sub>2</sub> nanocomposites with enhanced photocatalytic activity. *Molecules* **2019**, *24*, 2996. [[CrossRef](#)] [[PubMed](#)]
221. Lin, X.; Sun, M.; Gao, B.; Ding, W.; Zhang, Z.; Anandan, S.; Umar, A. Hydrothermally regulating phase composition of TiO<sub>2</sub> nanocrystals toward high photocatalytic activity. *J. Alloys Compd.* **2021**, *850*, 156653. [[CrossRef](#)]
222. Mohamed, M.A.; Jaafar, J.; Zain, M.F.M.; Minggu, L.J.; Kassim, M.B.; Salehmin, M.N.I.; Rosmi, M.S.; Salleh, W.N.; Othman, M.H.D. Concurrent growth, structural and photocatalytic properties of hybridized C, N co-doped TiO<sub>2</sub> mixed phase over g-C<sub>3</sub>N<sub>4</sub> nanostructured. *Scr. Mater.* **2018**, *142*, 143–147. [[CrossRef](#)]
223. Li, J.; Xu, X.; Liu, X.; Qin, W.; Wang, M.; Pan, L. Metal-organic frameworks derived cake-like anatase/rutile mixed phase TiO<sub>2</sub> for highly efficient photocatalysis. *J. Alloys Compd.* **2017**, *690*, 640–646. [[CrossRef](#)]
224. Peng, F.; Gao, H.; Zhang, G.; Zhu, Z.; Zhang, J.; Liu, Q. Synergistic effects of Sm and C co-doped mixed phase crystalline TiO<sub>2</sub> for visible light photocatalytic activity. *Materials* **2017**, *10*, 209. [[CrossRef](#)]
225. Jacob, K.A.; Peter, P.M.; Jose, P.E.; Balakrishnan, C.J.; Thomas, V.J. A simple method for the synthesis of anatase-rutile mixed phase TiO<sub>2</sub> using a convenient precursor and higher visible-light photocatalytic activity of Co-doped TiO<sub>2</sub>. *Mater. Today Proc.* **2021**, *49*, 1408–1417. [[CrossRef](#)]
226. Li, H.; Shen, X.; Liu, Y.; Wang, L.; Lei, J.; Zhang, J. Facile phase control for hydrothermal synthesis of anatase-rutile TiO<sub>2</sub> with enhanced photocatalytic activity. *J. Alloys Compd.* **2015**, *646*, 380–386. [[CrossRef](#)]
227. Wang, Q.; Qiao, Z.; Jiang, P.; Kuang, J.; Liu, W.; Cao, W. Hydrothermal synthesis and enhanced photocatalytic activity of mixed-phase TiO<sub>2</sub> powders with controllable anatase/rutile ratio. *Solid State Sci.* **2018**, *77*, 14–19. [[CrossRef](#)]
228. Yang, Z.; Wang, B.; Cui, H.; An, H.; Pan, Y.; Zhai, J. Synthesis of crystal-controlled TiO<sub>2</sub> nanorods by a hydrothermal method: Rutile and brookite as highly active photocatalysts. *J. Phys. Chem. C* **2015**, *119*, 16905–16912. [[CrossRef](#)]

229. Luthfiah, A.; Permana, M.D.; Deawati, Y.; Firdaus, M.L.; Rahayu, I.; Eddy, D.R. Photocatalysis of nanocomposite titania–natural silica as antibacterial against *Staphylococcus aureus* and *Pseudomonas aeruginosa*. *RSC Adv.* **2021**, *11*, 38528–38536. [[CrossRef](#)] [[PubMed](#)]
230. Duvarci, Ö.Ç.; Çiftçioğlu, M. Preparation and characterization of nanocrystalline titania powders by sonochemical synthesis. *Powder Technol.* **2012**, *228*, 231–240. [[CrossRef](#)]
231. Garibay-Febles, V.; Hernández-Pérez, I.; Arceo, L.D.B.; Meza-Espinoza, J.S.; Espinoza-Tapia, J.C.; González-Reyes, L. Microstructural study by electron microscopy of sonochemical synthesized TiO<sub>2</sub> nanoparticles. *Acta Microsc.* **2017**, *26*, 56–64.
232. Hernández-Pérez, I.; Maubert, A.M.; Rendón, L.; Santiago, P.; Herrera-Hernández, H.; Díaz-Barriga Arceo, L.; Garibay Febles, V.; Palacios Gonzalez, E.; González-Reyes, L. Ultrasonic synthesis: Structural, optical and electrical correlation of TiO<sub>2</sub> nanoparticles. *Int. J. Electrochem. Sci.* **2012**, *7*, 8832–8847.
233. Noman, M.T.; Militky, J.; Wiener, J.; Saskova, J.; Ashraf, M.A.; Jamshaid, H.; Azeem, M. Sonochemical synthesis of highly crystalline photocatalyst for industrial applications. *Ultrasonics* **2018**, *83*, 203–213. [[CrossRef](#)]
234. Arami, H.; Mazloumi, M.; Khalifehzadeh, R.; Sadrnezhad, S.K. Sonochemical preparation of TiO<sub>2</sub> nanoparticles. *Mater. Lett.* **2007**, *61*, 4559–4561. [[CrossRef](#)]
235. Ibrahim, A.; Mekprasart, W.; Pecharapa, W. Anatase/Rutile TiO<sub>2</sub> composite prepared via sonochemical process and their photocatalytic activity. *Mater. Today: Proc.* **2017**, *4*, 6159–6165.
236. Yu, J.C.; Zhang, L.; Yu, J. Direct sonochemical preparation and characterization of highly active mesoporous TiO<sub>2</sub> with a bicrystalline framework. *Chem. Mater.* **2002**, *14*, 4647–4653. [[CrossRef](#)]
237. Ozawa, T.; Iwasaki, M.; Tada, H.; Akita, T.; Tanaka, K.; Ito, S. Low-temperature synthesis of anatase–brookite composite nanocrystals: The junction effect on photocatalytic activity. *J. Colloid Interface Sci.* **2005**, *281*, 510–513. [[CrossRef](#)]
238. Matthews, A. The crystallization of anatase and rutile from amorphous titanium dioxide under hydrothermal conditions. *Am. Mineral.* **1976**, *61*, 419–424.
239. Hanaor, D.A.; Sorrell, C.C. Review of the anatase to rutile phase transformation. *J. Mater. Sci.* **2011**, *46*, 855–874. [[CrossRef](#)]
240. Sikong, L.; Damchan, J.; Kooptarnond, K.; Niyomwas, S. Effect of doped SiO<sub>2</sub> and calcinations temperature on phase transformation of TiO<sub>2</sub> photocatalyst prepared by sol-gel method. *Songklanakarin J. Sci. Technol.* **2008**, *30*, 385–391.
241. Pillai, S.C.; Periyat, P.; George, R.; McCormack, D.E.; Seery, M.K.; Hayden, H.; Colreavy, J.; Corr, D.; Hinder, S.J. Synthesis of High-Temperature Stable Anatase TiO<sub>2</sub> Photocatalyst. *J. Phys. Chem. C* **2007**, *111*, 1605–1611. [[CrossRef](#)]
242. Yuangpho, N.; Le, S.T.T.; Treerujiraphapong, T.; Khanitchaidecha, W.; Nakaruk, A. Enhanced photocatalytic performance of TiO<sub>2</sub> particles via effect of anatase–rutile ratio. *Physica E Low Dimens. Syst. Nanostruct.* **2015**, *67*, 18–22. [[CrossRef](#)]
243. Scarpelli, F.; Mastropietro, T.F.; Poerio, T.; Godbert, N. Mesoporous TiO<sub>2</sub> thin films: State of the art. In *Titanium Dioxide-Material for a Sustainable Environment*; Yang, D., Ed.; IntechOpen: London, UK, 2018; Volume 508, pp. 135–142.
244. Liu, L.; Zhao, H.; Andino, J.M.; Li, Y. Photocatalytic CO<sub>2</sub> reduction with H<sub>2</sub>O on TiO<sub>2</sub> nanocrystals: Comparison of anatase, rutile, and brookite polymorphs and exploration of surface chemistry. *ACS Catal.* **2012**, *2*, 1817–1828. [[CrossRef](#)]
245. Hurum, D.C.; Agrios, A.G.; Gray, K.A.; Rajh, T.; Thurnauer, M.C. Explaining the enhanced photocatalytic activity of Degussa P25 mixed-phase TiO<sub>2</sub> using EPR. *J. Phys. Chem. B* **2003**, *107*, 4545–4549. [[CrossRef](#)]
246. Mancinelli, R.; Botti, A.; Bruni, F.; Ricci, M.A.; Soper, A.K. Hydration of sodium, potassium, and chloride ions in solution and the concept of structure maker/breaker. *J. Phys. Chem. B* **2007**, *111*, 13570–13577. [[CrossRef](#)]
247. Zaw, Y.Y.; Channei, D.A.D.; Threrujirapapong, T.; Khanitchaidecha, W.; Nakaruk, A. Effect of anatase/rutile phase ratio on the photodegradation of methylene blue under uv irradiation. *Mater. Sci. Forum* **2020**, *998*, 78–83. [[CrossRef](#)]
248. Wetchakun, N.; Phanichphant, S. Effect of temperature on the degree of anatase–rutile transformation in titanium dioxide nanoparticles synthesized by the modified sol–gel method. *Curr. Appl. Phys.* **2008**, *8*, 343–346. [[CrossRef](#)]
249. Liu, Y.; Zou, X.; Li, L.; Shen, Z.; Cao, Y.; Wang, Y.; Cui, L.; Cheng, J.; Wang, Y.; Li, X. Engineering of anatase/rutile TiO<sub>2</sub> heterophase junction via in-situ phase transformation for enhanced photocatalytic hydrogen evolution. *J. Colloid Interface Sci.* **2021**, *599*, 795–804. [[CrossRef](#)] [[PubMed](#)]
250. Bakardjieva, S.; Šubrt, J.; Štengl, V.; Dianež, M.J.; Sayagues, M.J. Photoactivity of anatase–rutile TiO<sub>2</sub> nanocrystalline mixtures obtained by heat treatment of homogeneously precipitated anatase. *Appl. Catal. B* **2005**, *58*, 193–202. [[CrossRef](#)]
251. Yaemsunthorn, K.; Kobielski, M.; Macyk, W. TiO<sub>2</sub> with tunable anatase-to-rutile nanoparticles ratios: How does the photoactivity depend on the phase composition and the nature of photocatalytic reaction? *ACS Appl. Nano Mater.* **2021**, *4*, 633–643. [[CrossRef](#)]
252. Xia, X.; Peng, S.; Bao, Y.; Wang, Y.; Lei, B.; Wang, Z.; Huang, Z.; Gao, Y. Control of interface between anatase TiO<sub>2</sub> nanoparticles and rutile TiO<sub>2</sub> nanorods for efficient photocatalytic H<sub>2</sub> generation. *J. Power Sources* **2018**, *376*, 11–17. [[CrossRef](#)]
253. Lei, Y.; Yang, Y.; Zhang, P.; Zhou, J.; Wu, J.; Li, K.; Wang, W.; Chen, L. Controllable one-step synthesis of mixed-phase TiO<sub>2</sub> nanocrystals with equivalent anatase/rutile ratio for enhanced photocatalytic performance. *Nanomaterials* **2021**, *11*, 1347. [[CrossRef](#)]
254. Bernardini, C.; Cappelletti, G.; Dozzi, M.V.; Selli, E. Photocatalytic degradation of organic molecules in water: Photoactivity and reaction paths in relation to TiO<sub>2</sub> particles features. *J. Photochem. Photobiol. A: Chem.* **2010**, *211*, 185–192. [[CrossRef](#)]
255. Bojinova, A.; Kralchevska, R.; Poulivos, I.; Dushkin, C. Anatase/rutile TiO<sub>2</sub> composites: Influence of the mixing ratio on the photocatalytic degradation of Malachite Green and Orange II in slurry. *Mater. Chem. Phys.* **2007**, *106*, 187–192. [[CrossRef](#)]
256. Cong, S.; Xu, Y. Explaining the high photocatalytic activity of a mixed phase TiO<sub>2</sub>: A combined effect of O<sub>2</sub> and crystallinity. *J. Phys. Chem. C* **2011**, *115*, 21161–21168. [[CrossRef](#)]

257. Ohno, T.; Sarukawa, K.; Matsumura, M. Crystal faces of rutile and anatase TiO<sub>2</sub> particles and their roles in photocatalytic reactions. *New J. Chem.* **2002**, *26*, 1167–1170. [[CrossRef](#)]
258. Zhang, Y.; Chen, J.; Li, X. Preparation and photocatalytic performance of anatase/rutile mixed-phase TiO<sub>2</sub> nanotubes. *Catal. Lett.* **2010**, *139*, 129–133. [[CrossRef](#)]
259. Almashhori, K.; Ali, T.T.; Saeed, A.; Alwafi, R.; Aly, M.; Al-Hazmi, F.E. Antibacterial and photocatalytic activities of controllable (anatase/rutile) mixed phase TiO<sub>2</sub> nanophotocatalysts synthesized via a microwave-assisted sol–gel method. *New J. Chem.* **2020**, *44*, 562–570. [[CrossRef](#)]
260. Xiong, J.; Zhang, M.; Cheng, G. Facile polyol-triggered anatase–rutile heterophase TiO<sub>2-x</sub> nanoparticles for enhancing photocatalytic CO<sub>2</sub> reduction. *J. Colloid Interface Sci.* **2020**, *579*, 872–877. [[CrossRef](#)] [[PubMed](#)]
261. Lin, H.; Li, L.; Zhao, M.; Huang, X.; Chen, X.; Li, G.; Yu, R. Synthesis of high-quality brookite TiO<sub>2</sub> single-crystalline nanosheets with specific facets exposed: Tuning catalysts from inert to highly reactive. *J. Am. Chem. Soc.* **2012**, *134*, 8328–8331. [[CrossRef](#)] [[PubMed](#)]
262. Khedr, T.M.; El-Sheikh, S.M.; Kowalska, E.; Abdeldayem, H.M. The synergistic effect of anatase and brookite for photocatalytic generation of hydrogen and diclofenac degradation. *J. Environ. Chem. Eng.* **2021**, *9*, 106566. [[CrossRef](#)]
263. Kandiel, T.A.; Feldhoff, A.; Robben, L.; Dillert, R.; Bahnemann, D.W. Tailored titanium dioxide nanomaterials: Anatase nanoparticles and brookite nanorods as highly active photocatalysts. *Chem. Mater.* **2010**, *22*, 2050–2060. [[CrossRef](#)]
264. Shen, X.; Zhang, J.; Tian, B.; Anpo, M. Tartaric acid-assisted preparation and photocatalytic performance of titania nanoparticles with controllable phases of anatase and brookite. *J. Mater. Sci.* **2012**, *47*, 5743–5751. [[CrossRef](#)]
265. Shen, X.; Tian, B.; Zhang, J. Tailored preparation of titania with controllable phases of anatase and brookite by an alkaline hydrothermal route. *Catal. Today* **2013**, *201*, 151–158. [[CrossRef](#)]
266. Tay, Q.; Liu, X.; Tang, Y.; Jiang, Z.; Sum, T.C.; Chen, Z. Enhanced photocatalytic hydrogen production with synergistic two-phase anatase/brookite TiO<sub>2</sub> nanostructures. *J. Phys. Chem. C* **2013**, *117*, 14973–14982. [[CrossRef](#)]
267. El-Sheikh, S.M.; Khedr, T.M.; Zhang, G.; Vogiazzi, V.; Ismail, A.A.; O’Shea, K.; Dionysiou, D.D. Tailored synthesis of anatase–brookite heterojunction photocatalysts for degradation of cylindrospermopsin under UV–Vis light. *Chem. Eng. J.* **2017**, *310*, 428–436. [[CrossRef](#)]
268. Mutuma, B.K.; Shao, G.N.; Kim, W.D.; Kim, H.T. Sol–gel synthesis of mesoporous anatase–brookite and anatase–brookite–rutile TiO<sub>2</sub> nanoparticles and their photocatalytic properties. *J. Colloid Interface Sci.* **2015**, *442*, 1–7. [[CrossRef](#)] [[PubMed](#)]
269. Andrade-Guel, M.; Díaz-Jiménez, L.; Cortés-Hernández, D.; Cabello-Alvarado, C.; Ávila-Orta, C.; Bartolo-Pérez, P.; Gamero-Melo, P. Microwave assisted sol–gel synthesis of titanium dioxide using hydrochloric and acetic acid as catalysts. *Bol. Soc. Esp. Ceram. Vidr.* **2019**, *58*, 171–177. [[CrossRef](#)]
270. Quintero, Y.; Mosquera, E.; Dios, J.; García, A. Ultrasonic-assisted sol–gel synthesis of TiO<sub>2</sub> nanostructures: Influence of synthesis parameters on morphology, crystallinity, and photocatalytic performance. *J. Sol-Gel Sci. Technol.* **2020**, *94*, 477–485. [[CrossRef](#)]
271. Cihlar, J.; Kaspárek, V.; Kralova, M.; Castkova, K. Biphasic anatase–brookite nanoparticles prepared by sol–gel complex synthesis and their photocatalytic activity in hydrogen production. *Int. J. Hydrogen Energy* **2015**, *40*, 2950–2962. [[CrossRef](#)]
272. Cihlar, J.; Navarro, L.K.T.; Kaspárek, V.; Michalicka, J.; Cihlar Jr, J.; Kastyl, J.; Castkova, K.; Celko, L. Influence of LA/Ti molar ratio on the complex synthesis of anatase/brookite nanoparticles and their hydrogen production. *Int. J. Hydrogen Energy* **2021**, *46*, 8578–8593. [[CrossRef](#)]
273. Di Paola, A.; Cufalo, G.; Addamo, M.; Bellardita, M.; Campostrini, R.; Ischia, M.; Ceccato, R.; Palmisano, L. Photocatalytic activity of nanocrystalline TiO<sub>2</sub> (brookite, rutile and brookite-based) powders prepared by thermohydrolysis of TiCl<sub>4</sub> in aqueous chloride solutions. *Colloids Surf. A Physicochem. Eng. Asp.* **2008**, *317*, 366–376. [[CrossRef](#)]
274. Luo, B.; Li, Z.; Xu, Y. The positive effect of anatase and rutile on the brookite-photocatalyzed degradation of phenol. *RSC Adv.* **2015**, *5*, 105999–106004. [[CrossRef](#)]
275. Xu, H.; Zhang, L. Controllable one-pot synthesis and enhanced photocatalytic activity of mixed-phase TiO<sub>2</sub> nanocrystals with tunable brookite/rutile ratios. *J. Phys. Chem. C* **2009**, *113*, 1785–1790. [[CrossRef](#)]
276. Cao, Y.; Li, X.; Bian, Z.; Fuhr, A.; Zhang, D.; Zhu, J. Highly photocatalytic activity of brookite/rutile TiO<sub>2</sub> nanocrystals with semi-embedded structure. *Appl. Catal. B* **2016**, *180*, 551–558. [[CrossRef](#)]
277. Kim, M.G.; Lee, J.E.; Kim, K.S.; Kang, J.M.; Lee, J.H.; Kim, K.H.; Cho, M.; Lee, S.G. Photocatalytic degradation of methylene blue under UV and visible light by brookite–rutile bi-crystalline phase of TiO<sub>2</sub>. *New J. Chem.* **2021**, *45*, 3485–3497. [[CrossRef](#)]
278. Qi, L.; Liu, Y.; Li, C. Controlled synthesis of TiO<sub>2</sub>-B nanowires and nanoparticles for dye-sensitized solar cells. *Appl. Surf. Sci.* **2010**, *257*, 1660–1665. [[CrossRef](#)]
279. Wang, G.; Wang, Q.; Lu, W.; Li, J. Photoelectrochemical study on charge transfer properties of TiO<sub>2</sub>-B nanowires with an application as humidity sensors. *J. Phys. Chem. B* **2006**, *110*, 22029–22034. [[CrossRef](#)] [[PubMed](#)]
280. Feist, T.P.; Davies, P.K. The soft chemical synthesis of TiO<sub>2</sub> (B) from layered titanates. *J. Solid State Chem.* **1992**, *101*, 275–295. [[CrossRef](#)]
281. Yamamoto, K.; Tomita, K.; Fujita, K.; Kobayashi, M.; Petrykin, V.; Kakihana, M. Synthesis of TiO<sub>2</sub> (B) using glycolato titanium complex and post-synthetic hydrothermal crystal growth of TiO<sub>2</sub> (B). *J. Cryst. Growth* **2009**, *311*, 619–622. [[CrossRef](#)]
282. Kobayashi, M.; Petrykin, V.V.; Kakihana, M.; Tomita, K.; Yoshimura, M. One-step synthesis of TiO<sub>2</sub> (B) nanoparticles from a water-soluble titanium complex. *Chem. Mater.* **2007**, *19*, 5373–5376. [[CrossRef](#)]

283. Giannuzzi, R.; Manca, M.; De Marco, L.; Belviso, M.R.; Cannavale, A.; Sibillano, T.; Giannini, C.; Cozzoli, P.D.; Gigli, G. Ultrathin TiO<sub>2</sub> (B) nanorods with superior lithium-ion storage performance. *ACS Appl. Mater. Interfaces* **2014**, *6*, 1933–1943. [[CrossRef](#)]
284. Cai, J.; Wang, Y.; Zhu, Y.; Wu, M.; Zhang, H.; Li, X.; Jiang, Z.; Meng, M. In situ formation of disorder-engineered TiO<sub>2</sub> (B)-anatase heterophase junction for enhanced photocatalytic hydrogen evolution. *ACS Appl. Mater. Interfaces* **2015**, *7*, 24987–24992. [[CrossRef](#)]
285. Mikrut, P.; Kobielski, M.; Indyka, P.; Macyk, W. Photocatalytic activity of TiO<sub>2</sub> polymorph B revisited: Physical, redox, spectroscopic, and photochemical properties of TiO<sub>2</sub> (B)/anatase series of titanium dioxide materials. *Mater. Today Sustain.* **2020**, *10*, 100052. [[CrossRef](#)]
286. Zhu, J.; Zhu, S.; Kong, X.; Liang, Y.; Li, Z.; Wu, S.; Luo, S.; Chang, C.; Cui, Z. Rutile-coated B-phase TiO<sub>2</sub> heterojunction nanobelts for photocatalytic H<sub>2</sub> evolution. *ACS Appl. Nano Mater.* **2020**, *3*, 10349–10359. [[CrossRef](#)]
287. Chalastara, K.; Guo, F.; Elouatik, S.; Demopoulos, G.P. Tunable composition aqueous-synthesized mixed-phase TiO<sub>2</sub> nanocrystals for photo-assisted water decontamination: Comparison of anatase, brookite and rutile photocatalysts. *Catalysts* **2020**, *10*, 407. [[CrossRef](#)]
288. Allen, N.S.; Mahdjoub, N.; Vishnyakov, V.; Kelly, P.J.; Kriek, R.J. The effect of crystalline phase (anatase, brookite and rutile) and size on the photocatalytic activity of calcined polymorphic titanium dioxide (TiO<sub>2</sub>). *Polym. Degrad. Stab.* **2018**, *150*, 31–36. [[CrossRef](#)]
289. Kaplan, R.; Erjavec, B.; Dražić, G.; Grdadolnik, J.; Pintar, A. Simple synthesis of anatase/rutile/brookite TiO<sub>2</sub> nanocomposite with superior mineralization potential for photocatalytic degradation of water pollutants. *Appl. Catal. B* **2016**, *181*, 465–474. [[CrossRef](#)]

**Disclaimer/Publisher's Note:** The statements, opinions and data contained in all publications are solely those of the individual author(s) and contributor(s) and not of MDPI and/or the editor(s). MDPI and/or the editor(s) disclaim responsibility for any injury to people or property resulting from any ideas, methods, instructions or products referred to in the content.